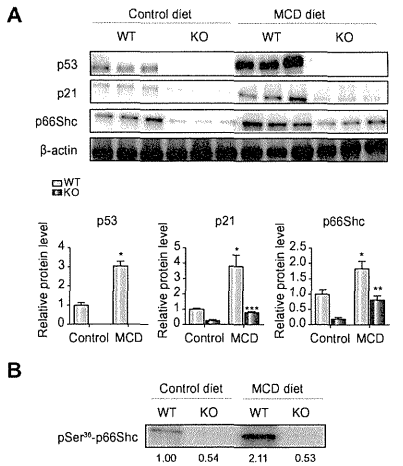

Fig. 2. p53 deficiency suppresses the enhancement of hepatic p66Shc signaling in nutritional steatohepatitis. (A) Western blot analysis of hepatic p53, p21, and p66Shc protein levels (upper panels), and quantification of the expression levels (lower panels) in the indicated groups, which were fed the MCD or control diet for 8 weeks. *p <0.05 compared with wild type mice fed the control diet, **p <0.05 compared with wild type mice fed the MCD diet, and ***p <0.05 compared with the other groups. (B) Immunoprecipitation analysis of hepatic p66Shc phosphorylated at Ser^{36} in the indicated groups. Relative protein levels were used to quantify changes relative to results from wild type mice fed the control diet, and are shown below each blot. KO, p53-deficient mice; WT, wild type mice.

p53 deficiency suppresses the enhancement of hepatic p66Shc signaling in nutritional steatohepatitis

We next examined hepatic p53 signaling in mice with nutritional steatohepatitis. Hepatic protein expression levels of p53 and p21 (a protein downstream of p53) significantly increased in mice with nutritional steatohepatitis compared with mice fed the control diet (Fig. 2A). Because p66Shc is associated with aging and oxidative stress [13] and functions downstream of p53 [14], we next examined hepatic p66Shc signaling. The levels of total p66Shc and p66Shc phosphorylated at Ser 36 in the liver were significantly enhanced in the mouse NASH model (Fig. 2A and B). After 8 weeks of MCD diet, a lack of p53 reduced the enhanced expression to the levels observed in wild type mice fed the control diet or lower (Fig. 2A and B). These results suggest that hepatic p21 and p66Shc signaling in the mouse model of NASH is mainly regulated by p53 signaling.

Deficiency of p53 reverses TGF-β-induced enhancement of p66Shc signaling and suppresses TGF-β-induced ROS accumulation in hepatocytes

Hepatic levels of p53 and p66Shc proteins in the MCD diet-fed mice significantly increased 3 weeks after treatment, and continued to rise until 8 weeks after treatment (Supplementary Fig. 1A). At the same time, hepatic TGF-β levels rose until 8 weeks after treatment in the MCD diet-fed mice compared with those in mice fed the control diet (Supplementary Fig. 1B). Lipid peroxidation was also significantly enhanced in the liver of mice with nutritional steatohepatitis after 8 weeks of MCD diet (Supplementary Fig. 1B). Besides TGF-β and ROS, TNFα is reportedly involved in the pathogenesis of NASH [15,16]; however, hepatic TNFα expression in mice fed the MCD diet peaked 3 weeks after treatment, and then decreased until 8 weeks after treatment (Supplementary Fig. 1B).

Additionally, TGF-β significantly increased p53 protein levels in primary cultured hepatocytes (Fig. 3A and B), whereas treatment with H_2O_2 or TNFα did not produce notable effects (Supplementary Fig. 1C and D). These results suggest that TGF-β contributes to the upregulation of p53 signaling in MCD diet-induced steatohepatitis. Furthermore, previous reports have shown that ROS, TGF-β, and the feedback between these signals play key roles in the pathogenesis of NASH [11,12]. Therefore, we detailed the relationships among TGF-β, ROS, and p53 and p66Shc signaling in hepatocytes.

TGF-β significantly enhanced the levels of p21, p66Shc, and p66Shc phosphorylated at Ser36 in hepatocytes (Fig. 3A and B). p53 deficiency or inactivation of p53 with the reversible p53 inhibitor pifithrin (PFT)-α reversed the TGF-β-induced changes in the levels of these proteins in hepatocytes (Fig. 3A and B). We also confirmed that PFT-α significantly lowered nuclear levels of p53, resulting in decreased p53 signaling (Fig. 3B).

Measures of protein carbonyls showed that TGF-β significantly increased ROS levels in primary cultured hepatocytes, whereas p53 deficiency prevented this effect (Fig. 3C). Inactivation of p53 with PFT-α also significantly suppressed TGF-β-induced ROS accumulation in hepatocytes (Fig. 3C). Similarly, quantification of MDA levels in hepatocyte cultures showed that blocking p53 signaling significantly decreased TGF-β-induced lipid peroxidation in hepatocytes (Fig. 3D).

p53 deficiency inhibits TGF-β-induced apoptosis in hepatocytes

Because TGF-β induces hepatocyte apoptosis via ROS generation [17,18], we performed *in vitro* TUNEL analysis using an enzyme-linked immunosorbent assay kit. The present result shows that TGF-β enhances apoptosis in primary cultured hepatocytes, while p53 deficiency or co-treatment with PFT-α ameliorates this effect (Fig. 3E and F). TGF-β treatment also significantly enhances caspase-3 activity in primary cultured hepatocytes. Deficiency or inactivation of p53 signaling results in significant inhibition of TGF-β-induced caspase-3 activity (Fig. 3E and F).

Increased hepatic expression of p53 and p21 in patients with NASH correlates with increased p66Shc expression

We next examined hepatic p53 and p66Shc signaling in human NASH. Using mRNA samples and paraffin-embedded tissue sections prepared from human liver biopsies performed to diagnose non-alcoholic fatty liver (NAFLD) or human non-tumorous normal liver samples obtained during surgery for colorectal liver metastases, we examined hepatic *p21* and *p66Shc* mRNA levels by real-time PCRs and hepatic p53 and p66Shc protein levels by immunohistochemistry. The mRNA expression levels of *p21* and *p66Shc* (Fig. 4A), and the protein expression levels of p53 and p66Shc (Fig. 4B and C) were significantly elevated in NAFLD liver samples, in comparison with those in normal liver samples. Among NAFLD patients, the NASH group showed significantly higher hepatic mRNA expression levels of *p21* and *p66Shc* (Fig. 4D), and significantly higher hepatic p53 and p66Shc protein levels (Fig. 4E) compared with the simple steatosis group. When we analyzed the relationship between hepatic expression levels of p53, p21, and p66Shc and the histological stage of fibrosis in NAFLD patients, we observed a stepwise increase with the increasing severity of hepatic fibrosis ($p = 0.0014$ for *p21* mRNA, $p = 0.0255$ for *p66Shc* mRNA, $p = 0.0005$ for p53 protein, $p < 0.0001$ for p66Shc protein by Kruskal–Wallis test) (Fig. 4F). There were significant differences in hepatic mRNA expression of *p21* between F0 and F1, F0 and F2, F0 and F3 ($p = 0.0191$, 0.0016, and 0.0005, respectively) (Fig. 4F). There were also significant differences in hepatic mRNA expression of *p66Shc* between F0 and F1, F0 and F2, F0 and F3 ($p = 0.0043$, 0.0102, and 0.0077, respectively) (Fig. 4F). Furthermore, we detected significant differences in hepatic p53 protein levels between F0 and F3 samples, and between F1–2 and F3 samples ($p = 0.0007$ and 0.0010, respectively). We also detected significant differences in hepatic protein expression of p66Shc between F0 and F1–2, F0 and F3, F1–2 and F3 samples ($p = 0.0018$, 0.0008, and 0.0010, respectively) (Fig. 4F). In addition, we detected significant correlations between *p21* and *p66Shc* mRNA levels, and between p53 and p66Shc protein levels (Fig. 4G).

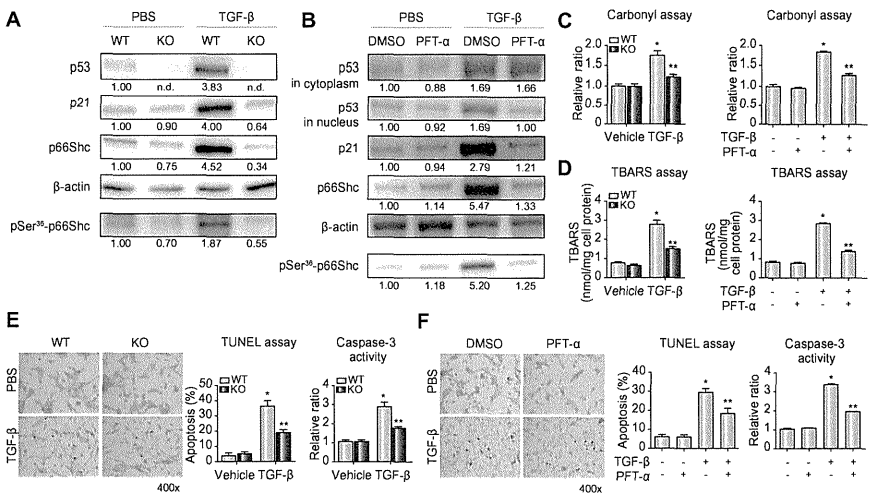

Fig. 3. Interrupting p53 signaling inhibits TGF-β-induced p66Shc signaling, ROS accumulation, and hepatocyte apoptosis. We examined hepatocyte cultures as previously described [12,17,18]. Protein levels of p53, p21, p66Shc, and phosphorylated p66Shc at Ser 36 (A) in primary cultured wild type (WT) or p53-deficient (KO) hepatocytes, exposed to TGF-β or not, and (B) in primary cultured WT hepatocytes, exposed to TGF-β with or without PFT-α. Relative protein levels (other than p66Shc phosphorylated at Ser 36, all protein levels were normalized to β-actin levels) were used to quantify changes relative to results from WT hepatocytes not treated with TGF-β or PFT-α, and are shown below each blot. Protein carbonyl levels (C) and MDA levels (D) in primary cultured WT or KO hepatocytes with or without TGF-β treatment (left panel), and in primary cultured WT hepatocytes exposed to TGF-β with or without PFT-α (right panel). The levels of protein carbonyls were normalized to results from WT hepatocytes without TGF-β or PFT-α. Means ± SEM from four individual experiments are shown. *p <0.05 compared with control levels. **p <0.05 compared with levels in WT hepatocytes after incubation with TGF-β but not PFT-α. (E, F) Representative images of TUNEL assays, apoptotic index values, and caspase-3 activity were obtained (E) for primary cultured WT or KO hepatocytes with or without TGF-β treatment, and (F) for primary cultured WT hepatocytes exposed to TGF-β with or without PFT-α. Caspase-3 activity was normalized to results from WT hepatocytes cultures without TGF-β or PFT-α. Means ± SEM from four individual experiments are shown. *p <0.05 compared with control group. **p <0.05 compared with results from WT hepatocytes after incubation with TGF-β but not PFT-α. (This figures appears in color on the web).

Discussion

The tumor suppressor p53 mediates responses to stress and induces the expression of proteins involved in cell cycle arrest or apoptosis. Recent studies have shown that, in addition to controlling cell-fate decisions and suppressing tumor development, p53 contributes to implantation, metabolism, and aging [5]. Some reports have examined the roles of p53 in liver diseases. For instance, inhibition of p53-dependent apoptosis reduced LPS-induced liver injury [19]. A recent report showed that p53 activation correlated with susceptibility to ethanol-induced liver damage, a pathologic condition that is thought to mechanistically resemble NASH [20]. In addition, hepatic p53 expression and hepatocyte apoptosis increase in patients with NASH and a mouse model of NASH [7,8]. These results suggest that p53 plays a role in the pathophysiology of NASH, although the precise contributions have not been fully elucidated.

In the present study, we examine p53 signaling in a mouse model of NASH induced by an MCD diet. In the nutritional

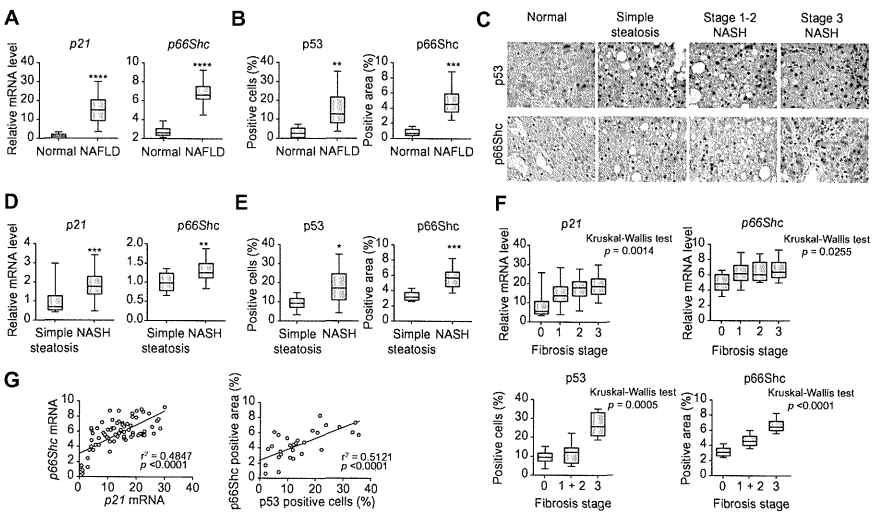

Fig. 4. Increased hepatic expression of p53 and p21 in patients with NASH correlates with increased p66Shc expression. (A) Hepatic mRNA levels of *p21* and *p66Shc* in 70 patients with NAFLD and 10 control subjects. ****p <0.0001 compared with the control group. (B) Hepatic p53 and p66Shc protein levels were immunohistochemically quantified in a subset of patients, including 5 control subjects, 8 patients with simple steatosis, 10 patients with stage 1–2 NASH, and 8 patients with stage 3 NASH. **p <0.01 and ***p <0.001 compared with the control group. (C) Immunohistochemically stained liver samples are representative of the indicated groups (400×). (D) Hepatic mRNA levels of *p21* and *p66Shc* in simple steatosis patients and NASH patients. **p <0.01 and ***p <0.001 compared with the simple steatosis group. (E) Hepatic protein levels of p53 and p66Shc in simple steatosis patients and NASH patients. *p <0.05 and ***p <0.001 compared with the simple steatosis group. (F) Hepatic *p21* and *p66Shc* mRNA levels, and hepatic p53 and p66Shc protein levels of each stage of liver fibrosis in NAFLD patients. Box plots demonstrate the interquartile range (box) as well as median and range. (G) Analysis of correlations between *p21* and *p66Shc* mRNA levels, and between p53 and p66Shc protein levels. (This figures appears in color on the web).

steatohepatitis, hepatic p53 signaling is enhanced and inhibition of p53 expression significantly ameliorates the pathologic manifestations of NASH. We use p53-deficient mice and PFT-α to analyze the roles of p53 in NASH. PFT-α selectively inhibits p53 transcriptional activity in various mouse cell lines, and prevents DNA damage-induced apoptosis in these cells [21].

ROS and TGF-β signaling in the liver are thought to play key roles in the pathogenesis of non-alcoholic steatohepatitis [11]. Our previous report also showed that ROS production and TGF-β expression in the mouse liver were significantly enhanced at every stage of nutritional steatohepatitis [12]. In addition, our present results show that TGF-β could play a central role in the upregulation of p53 signaling pathway in a mouse model of NASH, while p53 deficiency significantly inhibits ROS accumulation and reduces TGF-β expression in this NASH model. ROS in the liver activate hepatic non-parenchymal cells, including hepatic stellate cells, Kupffer cells, and endothelial cells [22]. Activated non-parenchymal cells release TGF-β, a profibrotic factor that has been implicated in autocrine or paracrine activation of hepatic stellate cells [23,24]. Hepatic stellate cells contribute to liver fibrosis; activated by stimuli as ROS and TGF-β, these cells produce collagen and additional TGF-β, leading to further activation of hepatic stellate cells via paracrine or autocrine mechanisms [25].

In a mouse model of NASH, hepatic p53 and p66Shc signaling was enhanced, and p53 deficiency suppressed the increase in p66Shc signaling in the liver. A previous study reported that p66Shc contributed to the regulation of cellular ROS levels and apoptosis as a downstream of p53 [14]. In addition, our *in vitro* experiments showed that TGF-β administration enhanced ROS levels and p66Shc signaling in hepatocytes. We also demonstrated that interrupting p53 signaling inhibited p66Shc activity and suppressed TGF-β-induced ROS accumulation in hepatocytes. Therefore, we hypothesized that ROS accumulation in hepatocytes was regulated by p53/p66Shc signaling to play a key role in NASH pathogenesis.

In the present study, we also showed that p53 deficiency ameliorated hepatocyte apoptosis in a mouse model of NASH. *In vitro* analysis also demonstrated that p53 deficiency inhibited TGF-β-induced apoptosis in primary cultured hepatocytes. These results implicate TGF-β-induced, p53-dependent apoptosis in the pathology of nutritional steatohepatitis.

In recent years, the signaling adapter protein p66Shc has received significant attention as a major determinant of cell resistance to oxidative stress and oxidant-induced cell damage and death [13,26]. p66Shc was also shown to play a pivotal role in impaired liver regeneration in older mice by inducing oxidative stress and apoptosis immediately after hepatectomy [13]. Our study showed that TGF-β enhanced p66Shc activity in hepatocytes via activation of p53 signaling. Taken together, these results suggest that TGF-β-induced hepatocyte injury in NASH may result from a cycle of p53 activation, enhanced p66Shc activities, and ROS accumulation, leading to apoptosis. In addition, our analysis of human samples demonstrated that enhanced p53/p66Shc signaling plays an important role in the progression of human NAFLD.

A previous study reported that IL-6/STAT3 pathway was positively correlated with hepatic expression of p21 [27]. In addition, TGF-β induced *p21* promoter activation in human hepatoma cells [28]. These reports suggest the possibility that the significant correlation between hepatic expression levels of p21 and p66Shc in our human samples might be in part due to increased expression of IL-6 and TGF-β during hepatic inflammation. Further studies using human samples are needed to fully elucidate the mechanisms.

In summary, we demonstrated that disrupted p53 signaling in hepatocytes ameliorated the progression of nutritional steatohepatitis. p53 signaling plays a pivotal role in the pathology-regulating mechanism, which is initiated by ROS that accumulate due to exaggeration of p66Shc activity in hepatocytes. Because p53 may regulate the susceptibility to NASH, future genetic and proteomic analyses may provide important insights.

There are no established therapeutic strategies for NASH, and effective treatments are urgently needed. Suppression of the p53/p66Shc signaling in the liver provides a promising target for the treatment of NASH.

Conflict of interest

The authors who have taken part in this study declared that they do not have anything to declare regarding funding from industry or conflict of interest with respect to this manuscript.

Acknowledgements

This study was supported by a grant from the National Defense Medical College, and the Ministry of Education, Culture, Sports, Science, and Technology of Japan.

Supplementary data

Supplementary data associated with this article can be found, in the online version, at http://dx.doi.org/10.1016/j.jhep.2012.05. 013.

References

[1] Neuschwander-Tetri BA. Fatty liver and the metabolic syndrome. Curr Opin Gastroenterol 2007;23:193–198.
[2] Falck-Ytter Y, Younossi ZM, Marchesini G, McCullough AJ. Clinical features and natural history of non-alcoholic steatosis syndromes. Semin Liver Dis 2001;21:17–26.
[3] Adams LA, Lymp JF, St. Sauver J, Sanderson SO, Lindor KD, Feldstein A, et al. The natural history of non-alcoholic fatty liver disease: a population-based cohort study. Gastroenterology 2005;129:113–121.
[4] Estep JM, Birerdinc A, Younossi Z. Non-invasive diagnostic tests for non-alcoholic fatty liver disease. Curr Mol Med 2010;10:166–172.
[5] Lu X. Tied up in loops: positive and negative autoregulation of p53. Cold Spring Harb Perspect Biol 2010;2:a000984.
[6] Hwang PM, Bunz F, Yu J, Rago C, Chan TA, Murphy MP, et al. Ferredoxin reductase affects p53-dependent, 5-fluorouracil-induced apoptosis in colorectal cancer cells. Nat Med 2001;7:1111–1117.
[7] Panasiuk A, Dzieciol J, Panasiuk B, Prokopowicz D. Expression of p53, Bax and Bcl-2 proteins in hepatocytes in non-alcoholic fatty liver disease. World J Gastroenterol 2006;12:6198–6202.
[8] Farrell GC, Larter CZ, Hou JY, Zhang RH, Yeh MM, Williams J, et al. Apoptosis in experimental NASH is associated with p53 activation and TRAIL receptor expression. J Gastroenterol Hepatol 2009;24:443–452.
[9] Leclercq IA, Farrell GC, Field J, Bell DR, Gonzalez FJ, Robertson GR. CYP2E1 and CYP4A as microsomal catalysts of lipid peroxides in murine non-alcoholic steatohepatitis. J Clin Invest 2000;105:1067–1075.
[10] Ribeiro PS, Cortez-Pinto H, Sola S, Castro RE, Ramalho RM, Baptista A, et al. Hepatocyte apoptosis, expression of death receptors, and activation of NF-kappaB in the liver of non-alcoholic and alcoholic steatohepatitis patients. Am J Gastroenterol 2004;99:1708–1717.
[11] Day CP. Genes or environment to determine alcoholic liver disease and non-alcoholic fatty liver disease. Liver Int 2006;26:1021–1028.
[12] Tomita K, Oike Y, Teratani T, Taguchi T, Noguchi M, Suzuki T, et al. Hepatic AdipoR2 signaling plays a protective role against progression of non-alcoholic steatohepatitis in mice. Hepatology 2008;48:458–473.
[13] Haga S, Morita N, Irani K, Fujiyoshi M, Ogino T, Ozawa T, et al. P66(Shc) has a pivotal function in impaired liver regeneration in aged mice by a redox-dependent mechanism. Lab Invest 2010;90:1718–1726.
[14] Trinei M, Giorgio M, Cicalese A, Barozzi S, Ventura A, Migliaccio E, et al. A p53–p66Shc signalling pathway controls intracellular redox status, levels of oxidation-damaged DNA and oxidative stress-induced apoptosis. Oncogene 2002;21:3872–3878.
[15] Tomita K, Tamiya G, Ando S, Ohsumi K, Chiyo T, Mizutani A, et al. Tumour necrosis factor alpha signalling through activation of Kupffer cells plays an essential role in liver fibrosis of non-alcoholic steatohepatitis in mice. Gut 2006;55:415–424.
[16] Koppe SW, Sahai A, Malladi P, Whitington PF, Green RM. Pentoxifylline attenuates steatohepatitis induced by the methionine choline deficient diet. J Hepatol 2004;41:592–598.
[17] Black D, Bird MA, Samson CM, Lyman S, Lange PA, Schrum LW, et al. Primary cirrhotic hepatocytes resist TGFbeta-induced apoptosis through a ROS-dependent mechanism. J Hepatol 2004;40:942–951.
[18] Black D, Lyman S, Qian T, Lemasters JJ, Rippe RA, Nitta T, et al. Transforming growth factor beta mediates hepatocyte apoptosis through Smad3 generation of reactive oxygen species. Biochimie 2007;89:1464–1473.
[19] Schafer T, Scheuer C, Roemer K, Menger MD, Vollmar B. Inhibition of p53 protects liver tissue against endotoxin-induced apoptotic and necrotic cell death. FASEB J 2003;17:660–667.
[20] Derdak Z, Lang CH, Villegas KA, Tong M, Mark NM, de la Monte SM, et al. Activation of p53 enhances apoptosis and insulin resistance in a rat model of alcoholic liver disease. J Hepatol 2011;54:164–172.
[21] Komarov PG, Komarova EA, Kondratov RV, Christov-Tselkov K, Coon JS, Chernov MV, et al. A chemical inhibitor of p53 that protects mice from the side effects of cancer therapy. Science 1999;285:1733–1737.
[22] Poli G. Pathogenesis of liver fibrosis: role of oxidative stress. Mol Aspects Med 2000;21:49–98.
[23] Bissell DM, Wang SS, Jarnagin WR, Roll FJ. Cell-specific expression of transforming growth factor-beta in rat liver. Evidence for autocrine regulation of hepatocyte proliferation. J Clin Invest 1995;96:447–455.
[24] Matsuoka M, Tsukamoto H. Stimulation of hepatic lipocyte collagen production by Kupffer cell-derived transforming growth factor beta: implication for a pathogenetic role in alcoholic liver fibrogenesis. Hepatology 1990;11:599–605.
[25] Galli A, Svegliati-Baroni G, Ceni E, Milani S, Ridolfi F, Salzano R, et al. Oxidative stress stimulates proliferation and invasiveness of hepatic stellate cells via a MMP2-mediated mechanism. Hepatology 2005;41:1074–1084.
[26] Migliaccio E, Giorgio M, Mele S, Pelicci G, Reboldi P, Pandolfi PP, et al. The p66shc adaptor protein controls oxidative stress response and life span in mammals. Nature 1999;402:309–313.
[27] Torbenson M, Yang SQ, Liu HZ, Huang J, Gage W, Diehl AM. STAT-3 overexpression and p21 up-regulation accompany impaired regeneration of fatty livers. Am J Pathol 2002;161:155–161.
[28] Cheng PL, Chang MH, Chao CH, Lee YH. Hepatitis C viral proteins interact with Smad3 and differentially regulate TGF-beta/Smad3-mediated transcriptional activation. Oncogene 2004;23:7821–7838.

Genetic and Metabolic Diseases

A High-Cholesterol Diet Exacerbates Liver Fibrosis in Mice via Accumulation of Free Cholesterol in Hepatic Stellate Cells

TOSHIAKI TERATANI,* KENGO TOMITA,*,‡ TAKAHIRO SUZUKI,* TETSUYA OSHIKAWA,* HIROKAZU YOKOYAMA,§ KATSUYOSHI SHIMAMURA,* SUSUMU TOMINAGA,‖ SADAYUKI HIROI,‖ RIE IRIE,¶ YOSHIKIYO OKADA,‡ CHIE KURIHARA,‡ HIROTOSHI EBINUMA,* HIDETSUGU SAITO,# RYOTA HOKARI,‡ KAZUO SUGIYAMA,* TAKANORI KANAI,* SOICHIRO MIURA,‡ and TOSHIFUMI HIBI*

*Division of Gastroenterology and Hepatology, Department of Internal Medicine, §Health Center, Keio University School of Medicine, Tokyo, Japan; ‡Division of Gastroenterology and Hepatology, Department of Internal Medicine, ‖Department of Pathology and Laboratory Medicine, National Defense Medical College, Saitama, Japan; ¶Department of Pathology, Kawasaki Municipal Hospital, Kanagawa, Japan; #Graduate School of Pharmaceutical Sciences, Keio University Faculty of Pharmacy, Tokyo, Japan

See editorial on page 8.

BACKGROUND & AIMS: Some studies have indicated that dietary cholesterol has a role in the progression of liver fibrosis. We investigated the mechanisms by which dietary cholesterol might contribute to hepatic fibrogenesis. **METHODS:** C57BL/6 mice were fed a high-cholesterol diet or a control diet for 4 weeks; liver fibrosis then was induced by bile-duct ligation or carbon tetrachloride administration. Hepatic stellate cells (HSCs) were isolated from mice fed high-cholesterol diets or from Niemann-Pick type C1-deficient mice, which accumulate intracellular free cholesterol. **RESULTS:** After bile-duct ligation or carbon tetrachloride administration, mice fed high-cholesterol diets had significant increases in liver fibrosis and activation of HSCs compared with mice fed control diets. There were no significant differences in the degree of hepatocellular injury or liver inflammation, including hepatocyte apoptosis or Kupffer cell activation, between mice fed high-cholesterol or control diets. Levels of free cholesterol were much higher in HSCs from mice fed high-cholesterol diets than those fed control diets. In cultured HSCs, accumulation of free cholesterol in HSCs increased levels of Toll-like receptor 4 (TLR4), leading to down-regulation of bone morphogenetic protein and activin membrane-bound inhibitor (a pseudoreceptor for transforming growth factor [TGF]β); the HSCs became sensitized to TGFβ-induced activation. Liver fibrosis was not aggravated by the high-cholesterol diet in C3H/HeJ mice, which express a mutant form of TLR4; HSCs that express mutant TLR4 were not activated by accumulation of free cholesterol. **CONCLUSIONS: Dietary cholesterol aggravates liver fibrosis because free cholesterol accumulates in HSCs, leading to increased TLR4 signaling, down-regulation of bone morphogenetic protein and activin membrane-bound inhibitor, and sensitization of HSC to TGFβ. This pathway might be targeted by antifibrotic therapies.**

Keywords: Liver Disease; Mouse Model; Dyslipidemia; Lipopolysaccharide.

Liver fibrosis, a condition that indicates the progression of liver diseases, may progress to cirrhosis or hepatocellular carcinoma.[1] For this reason, it is important to thoroughly determine the pathologic mechanisms associated with this disorder.

Dietary factors are likely to be important determinants of liver fibrosis development. Data derived from 9221 participants in the first National Health and Nutrition Examination Survey in the United States showed that higher dietary consumption of cholesterol was associated with a higher risk of cirrhosis or liver cancer in both unadjusted and adjusted analyses.[2]

Several studies also have reported that statins and ezetimibe (cholesterol-lowering agents) improve liver fibrosis in patients with hypercholesterolemia.[3,4] In recent laboratory studies, rodents or rabbits developed liver fibrosis after long-term consumption of a high-cholesterol (HC) diet containing cholic acid (atherogenic diet) or a high-fat HC diet.[5,6] However, experiments using such diets are not suitable for explaining the exact role of cholesterol in the development of liver fibrosis because cholic acid and free fatty acids induce hepatic fibrosis genes,[7] hepatocyte apoptosis, and liver inflammation.[8] Although these studies are part of a growing accumulation of evidence showing the key role of cholesterol in the development and progression of liver fibrosis, the exact role of cholesterol in the mechanisms underlying liver fibrosis remains to be explored.

To clarify the precise impact of cholesterol in the pathophysiology of liver fibrosis, we therefore used experimental models involving administration of HC diets not containing cholic acid or an excessive amount of fatty acids to mice in which liver fibrosis was induced by bile duct ligation (BDL) or carbon tetrachloride (CCl_4) intoxication. Hepatic stellate cells (HSCs), the main producers of extracellular matrix in the fibrotic liver, play a key role in liver fibrosis, although liver fibrosis is strongly associated with some elements of liver injury, including hepatocyte death and Kupffer cell activation.[1] Our results show that consumption of an HC diet caused accumulation of free cholesterol in HSCs, which in turn significantly suppressed the expression of the transforming growth factor-β (TGFβ) pseudoreceptor bone morphogenetic protein and activin membrane-bound inhibitor (Bambi) through enhancement of Toll-like receptor 4 (TLR4) signaling, leading to aggravation of liver fibrosis.

Abbreviations used in this paper: AcLDL, acetyl low-density lipoprotein; ALT, alanine aminotransferase; Bambi, BMP and activin membrane-bound inhibitor; BDL, bile duct ligation; CCl_4, carbon tetrachloride; CE, cholesterol ester; compound 58035, acyl-CoA:cholesterol acyltransferase inhibitor 58035; FC, free cholesterol; HC, high cholesterol; HSCs, hepatic stellate cells; KO, knock-out; LPS, lipopolysaccharide; mRNA, messenger RNA; NPC1, Niemann-Pick type C1; αSMA, α-smooth muscle actin; TC, total cholesterol; TG, triglyceride; TGFβ, transforming growth factor β; TLR4, Toll-like receptor 4; TNFα, tumor necrosis factor-α; WT, wild-type.

© 2012 by the AGA Institute
0016-5085/$36.00
doi:10.1053/j.gastro.2011.09.049

Materials and Methods

Please refer to the Supplementary Materials and Methods section for more detailed descriptions.

Animal Model

Male 8-week-old wild-type (WT) C57BL/6, C3H/HeN, or C3H/HeJ mice were fed an HC (1% wt/wt) diet (TD 92181) or a corresponding control diet (Teklad no. 7001; Harlan Teklad, Madison, WI) for 4 weeks, and then either underwent BDL for 3 weeks, or were given CCl_4 at a dose of 5 μL (10% CCl_4 in corn oil)/g body weight, by intraperitoneal injection twice a week for 4 weeks.

Statistical Analysis

All data are expressed as the means ± standard errors of the means. Statistical analyses were performed using the unpaired Student t test or 1-way analysis of variance ($P < .05$ was considered significant).

Results

HC Diet Significantly Accelerated BDL- and CCl_4-Induced Liver Fibrosis

C57BL/6 mice were administered either an HC or control diet for 4 weeks and then divided into 2 groups: one group underwent BDL for 3 weeks and the other group received sham treatment. In a similar but separate experiment, mice were fed an HC or control diet for 4 weeks and then divided into 2 groups: one for 4-week treatment with CCl_4 and the other for treatment with corn oil.

The HC diet did not increase mean body or liver weight vs control (Supplementary Table 1). Although the HC diet significantly increased the serum concentration of total cholesterol (TC), no change was noted in serum triglyceride (TG) and glucose levels (Supplementary Table 1). In addition, the HC diet alone was not sufficient to cause hepatic steatosis or liver fibrosis (Figures 1 and 2). However, as shown by Masson trichrome staining and immunohistochemical staining of α-smooth muscle actin (αSMA) in liver tissue, as well as by liver hydroxyproline quantitative measurement results, BDL significantly exacerbated liver fibrosis in the HC diet group as compared with the control (Figures 1*A* and *B*). The messenger RNA (mRNA) expressions of collagen 1α1, collagen 1α2, and αSMA were significantly enhanced with the development of BDL-induced liver fibrosis, which was more evident in the HC diet group than in the control group (Figure 1*C*). TGFβ mRNA levels showed no significant differences between the diet groups (Figure 1*C*). In a similar manner to the BDL model, the murine CCl_4 model of liver fibrosis showed a significant progression of liver fibrosis in the HC diet group vs control (Figures 1*D* and *E*). The mRNA expression of collagen 1α1, collagen 1α2, and αSMA was significantly promoted as a result of the development of CCl_4-induced liver fibrosis, and this was seen more clearly in the HC diet group than in the control group (Figure 1*F*). TGFβ mRNA levels showed no significant between-group differences (Figure 1*F*).

HC Diet Did Not Accelerate BDL- or CCl_4-Induced Hepatocellular Damage

Hepatic TC levels were increased significantly by HC diet consumption for both the BDL and sham groups (Figure 2*A*). However, liver TG levels showed no significant difference between the HC and control groups, and HC diet did not cause hepatic steatosis (Figures 1*A* and 2*A*).

Serum alanine aminotransferase (ALT) levels, a biological marker of hepatocellular damage, were increased significantly in BDL-treated mice; however, this increase was not dependent on dietary cholesterol intake for either the sham or BDL group (Figure 2*B*). In addition, the HC diet did not significantly impact the mitochondrial inner membrane potentials or the numbers of terminal deoxynucleotidyl transferase–mediated deoxyuridine nick-end labeling-positive hepatocytes in the livers of BDL mice (Figure 2*C*).

Hepatic TC levels were increased significantly by consumption of the HC diet vs the control diet for both the CCl_4- and corn oil-treated groups (Figure 2*D*). However, liver TG levels showed no significant difference between the HC and control groups, and the HC diet did not cause hepatic steatosis (Figures 1*D* and 2*D*).

Treatment with CCl_4 significantly increased serum ALT levels relative to treatment with corn oil; however, consumption of the HC diet did not influence serum ALT levels in either the corn oil or CCl_4 group when compared with the control diet (Figure 2*E*). The HC diet did not significantly change the mitochondrial inner membrane potentials or the numbers of terminal deoxynucleotidyl transferase–mediated deoxyuridine nick-end labeling-positive hepatocytes in the livers of CCl_4-treated mice (Figure 2*F*).

In addition, the HC diet did not aggravate acute BDL- or CCl_4-induced hepatocellular damage, even at the time point when liver injury is known to peak (Supplementary Figures 1*A* and *B* and 2*A* and *B*).

These results show that the increase in hepatic cholesterol levels induced by intake of an HC diet did not aggravate BDL- or CCl_4-induced hepatocellular damage.

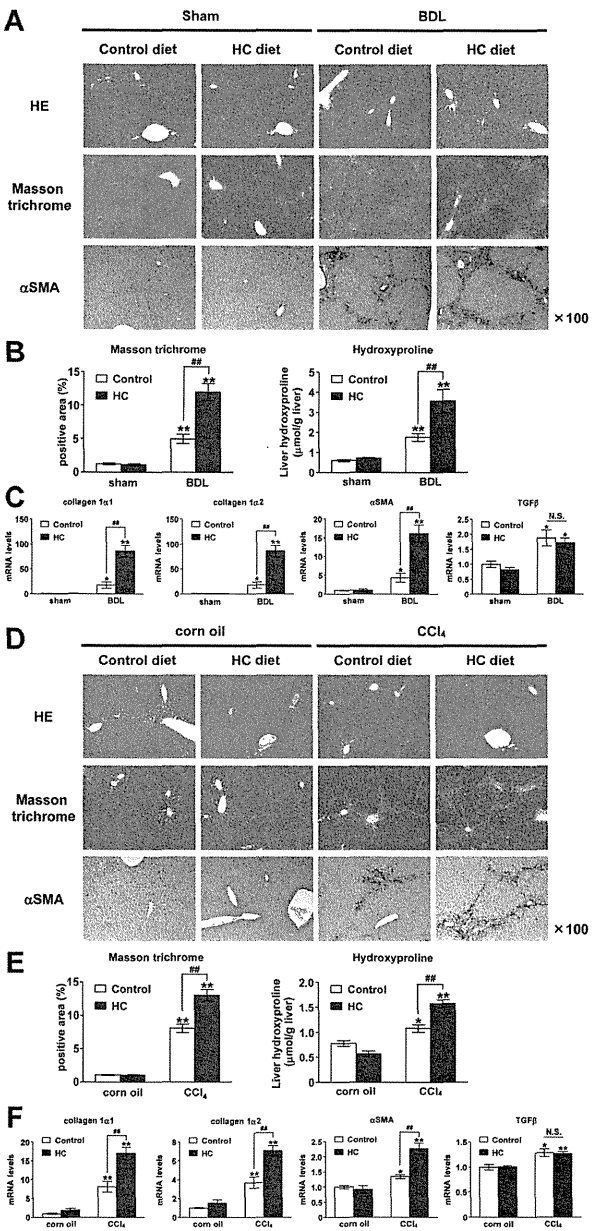

Figure 1. Effects of the HC diet on liver fibrosis induced by BDL or CCl_4 treatment. After being fed a control or HC diet for 4 weeks, C57BL/6 mice were subjected to (*A–C*) 3-week BDL or (*D–F*) CCl_4 treatment twice a week for 4 weeks to induce liver fibrosis (N = 5–7/group). (*A* and *D*) H&E-stained sections, Masson trichrome-stained sections, and immunohistochemical detection of αSMA in representative liver samples. (*B* and *E*) Quantification of Masson trichrome staining (left panel), and liver hydroxyproline concentrations (right panel). (*C* and *F*) Hepatic expression of collagen1α1, collagen1α2, αSMA, and TGFβ mRNA (N = 5/group). $^{*}P < .05$ and $^{**}P < .01$ compared with the (*B* and *C*) control diet–sham-operated group or the (*E* and *F*) control diet–corn oil group. $^{\#\#}P < .01$ compared with the (*B* and *C*) control diet-BDL group or the (*E* and *F*) control diet–CCl_4 group.

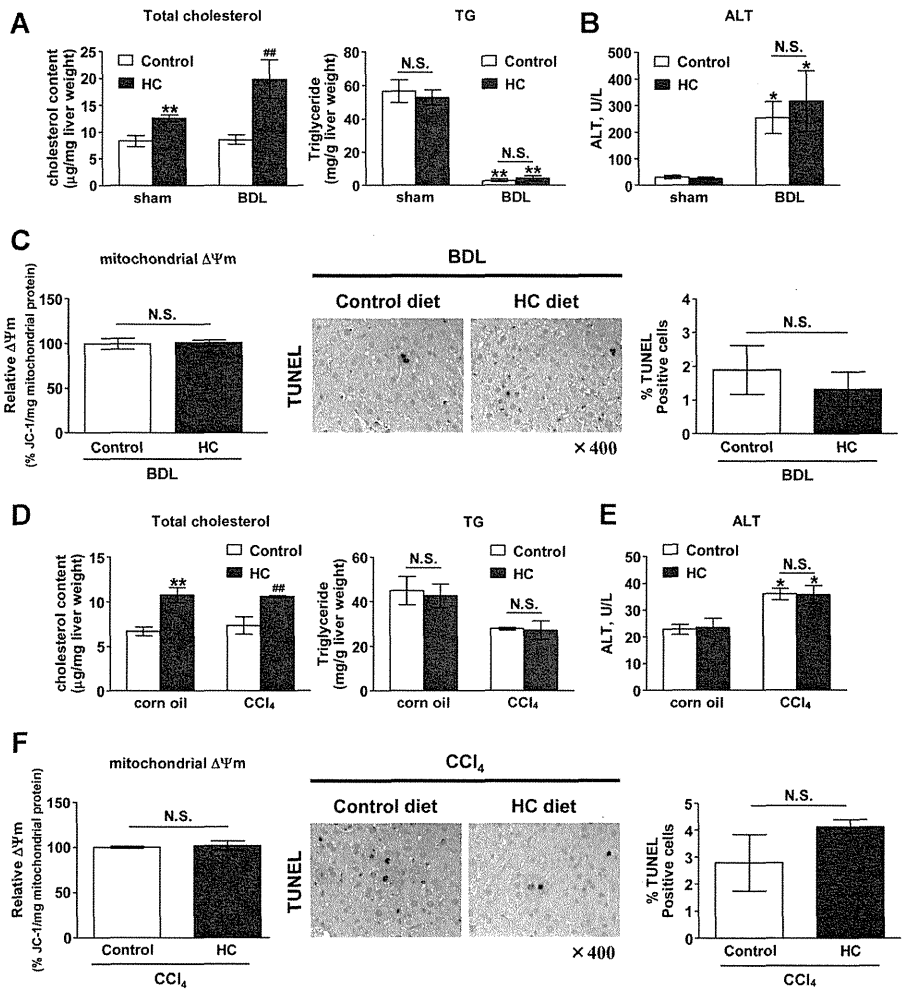

Figure 2. Effects of HC diet on hepatocyte injury induced by BDL or CCl_4 treatment. (*A* and *D*) Hepatic TC and TG contents (N = 5–7/group). (*B* and *E*) Serum ALT activities (N = 5–7/group). (*C* and *F*, *left panels*) Electrochemical proton gradient ($\Delta\Psi$) of the inner mitochondrial membrane (N = 5/group) (*C*, BDL-treated groups; *F*, CCl_4-treated groups). The calculated relative $\Delta\Psi$ was normalized to the values obtained in mice from the (*C*) control diet-BDL group or the (*F*) control diet-CCl_4 group. (*C* and *F*, *right panels*) The percentage of terminal deoxynucleotidyl transferase–mediated deoxyuridine nick-end labeling (TUNEL)-positive hepatocytes and the representative sections (N = 5–7/group). $^{*}P < .05$ and $^{**}P < .01$ compared with the (*A* and *B*) control diet–sham-operated group or the (*D* and *E*) control diet–corn oil group. $^{\#\#}P < .01$ compared with the (*A*) control diet-BDL group or the (*D*) control diet–CCl_4 group.

HC Diet Did Not Impact BDL- or CCl_4-Induced Kupffer Cell Activation or Liver Inflammation

Hepatic macrophage infiltration was evaluated by immunohistochemical staining using the Kupffer cell/macrophage marker F4/80 antibody. The results show BDL-enhanced infiltration of macrophages into the liver in both control- and HC-diet-fed mice. However, consumption of the HC diet did not influence this infiltration (Figure 3*A* and *B*). Kupffer cells are the major source of

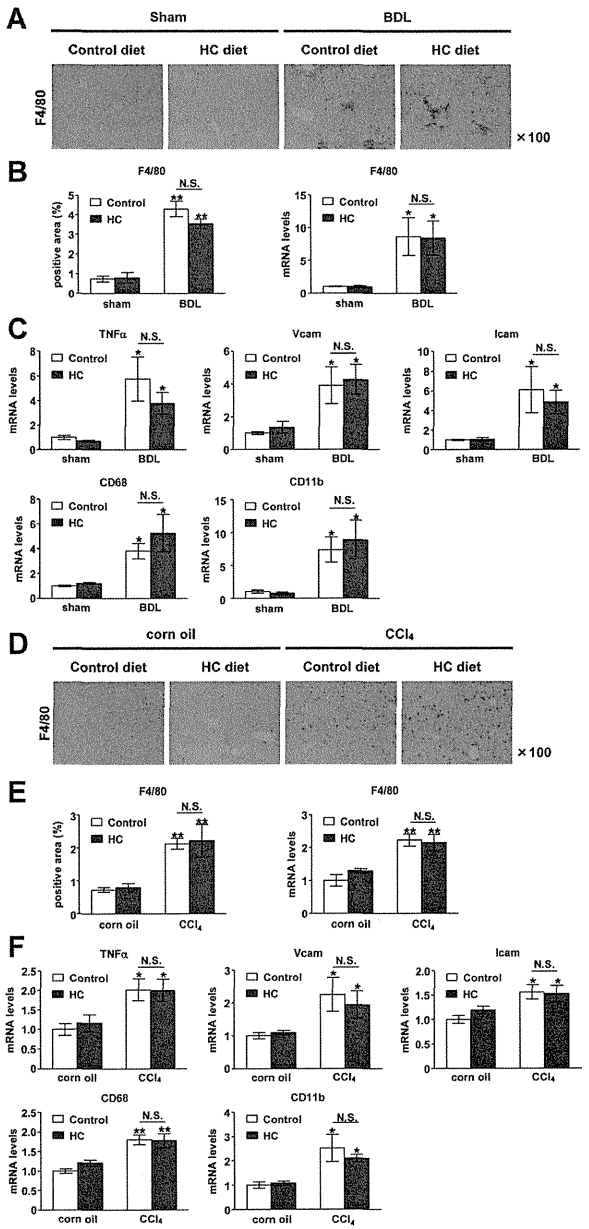

Figure 3. *Effects of HC diet on hepatic macrophage infiltration and Kupffer cell activation induced by BDL or CCl_4 treatment. (A and D)* Immunohistochemical detection of F4/80-positive cells in livers. *(B and E)* Quantification of F4/80 in immunohistochemical staining and mRNA. *(C and F)* Hepatic expression of TNFα, vascular cell adhesion molecule-1 (VCAM-1), intercellular adhesion molecule-1 (ICAM-1), CD68, and CD11b mRNA (N = 5/group). *(A–C)* Sham-operated or BDL groups, and *(D–F)* corn oil or CCl_4-treated groups. $^*P < .05$ and $^{**}P < .01$ compared with the *(B and C)* control diet–sham-operated group or the *(E and F)* control diet–corn oil group.

tumor necrosis factor-α (TNFα) production in the liver. Although BDL significantly promoted TNFα mRNA expression in the liver, the HC diet did not accelerate TNFα genetic expression. In addition, although BDL significantly increased mRNA expression of vascular cell adhesion molecule-1, intercellular adhesion molecule-1, CD68, and CD11b, this increase was not impacted by consumption of the HC diet (Figure 3*C*).

Mice treated with CCl_4 showed enhanced hepatic macrophage infiltration, similar to those treated with BDL. However, consumption of the HC diet did not impact the CCl_4-mediated hepatic macrophage infiltration (Figure 3*D* and *E*). Treatment with CCl_4 significantly increased hepatic levels of TNFα, vascular cell adhesion molecule-1, intercellular adhesion molecule-1, CD68, and CD11b mRNA; however, these levels were not influenced by HC diet consumption (Figure 3*F*). In addition, the HC diet did not influence acute BDL- or CCl_4-induced liver inflammation, even at the time point when liver inflammation peaks (Supplementary Figures 1*C–E* and 2*C–E*).

These results show that the HC diet used in this study did not influence the activation of Kupffer cells or the recruitment of macrophages to the liver. In addition, the HC diet did not impact the BDL- or CCl_4-mediated infiltration of inflammatory cells such as T cells and neutrophils into the liver (Supplementary Figure 3). H&E staining and immunohistochemical staining for CD68 also showed that the HC diet did not induce the formation of hepatic macrophage foam cells or cause liver inflammation (Figure 1*A* and *D* and Supplementary Figure 4).

HC Diet-Induced Aggravation of Liver Fibrosis Was Kupffer Cell–Independent

To determine whether the aggravation of liver fibrosis resulting from HC diet consumption required the presence of Kupffer cells, mice depleted of Kupffer cells with liposomal clodronate were treated with BDL or CCl_4 intoxication. In the BDL model, liposomal clodronate achieved almost complete depletion of Kupffer cells (Figure 4*A*), along with suppression of proinflammatory cytokines such as TNFα and interleukin-1β (Supplementary Figure 5*A*). Treatment with liposomal clodronate did not impact the BDL-induced hepatocellular injury (Figure 4*A*, bottom row). In mice treated with liposomal clodronate, intake of the HC diet significantly promoted the BDL-induced aggravation of liver fibrosis (Figure 4*B*). In agreement with these results, mice treated with liposomal clodronate showed a significant increase in BDL-induced expression of collagen 1α1, collagen 1α2, and αSMA in the liver when fed an HC diet (Figure 4*C*).

Similarly, treatment with liposomal clodronate almost completely depleted Kupffer cells in the CCl_4 model (Figure 4*D*), and also suppressed proinflammatory cytokines such as TNFα and interleukin-1β (Supplementary Figure 5*B*). Administration of liposomal clodronate did not impact the CCl_4-induced hepatocellular injury (Figure 4*D*, bottom row). In mice infused with liposomal clodronate, the HC diet significantly boosted the CCl_4-induced progression of liver fibrosis (Figure 4*E*). In accord with these findings, mice dosed with liposomal clodronate showed a significant increase in CCl_4-induced mRNA expression of collagen 1α1, collagen 1α2, and αSMA in the liver when administered the HC diet (Figure 4*F*).

These results suggested that the HC diet promoted BDL- and CCl_4-induced liver fibrosis in a Kupffer cell-independent manner.

Accumulation of Free Cholesterol Sensitized HSCs to TGFβ-Induced Activation

To examine the effects of the HC diet on HSCs, these cells were isolated from mice given the control or HC diets. With HSCs from the control diet group, the mean (±SD) TC content was 28.94 ± 11.55 μg/mg cell protein. In HSCs from the HC diet group, the mean (±SD) TC content was increased significantly to 59.90 ± 22.93 μg/mg cell protein. In addition, free cholesterol (FC) and cholesterol ester (CE) levels in HSCs were determined. Consequently, FC levels were significantly higher in the HC diet group HSCs than in those from the control diet group; however, no significant difference was noted in the CE level between groups (Figure 5*A*).

Second, to investigate the effects of HC diet on HSC activation, HSCs isolated from mice from both groups were stimulated with profibrogenic cytokine TGFβ. Samples of HSCs before treatment with TGFβ, collected from mice, showed that the HC diet did not affect mRNA levels of collagen 1α1, collagen 1α2, or αSMA. Treatment with TGFβ significantly enhanced the levels of collagen 1α1, collagen 1α2, and αSMA mRNA transcripts in HSCs. The enhancing effect was noted more prominently in the HC diet group than in controls (Figure 5*B*, top row). The HSC expression levels of TGFβ receptor-1 and TGFβ receptor-2 (regulating sensitivity to TGFβ) and the TGFβ pseudoreceptor Bambi were compared quantitatively between the 2 diet groups. Expression of Bambi was significantly lower in the HC diet group than the control group (Figure 5*B*, bottom row), however, no significant difference was observed in the expression levels of the TGFβ receptors between groups. In accord with these findings, hepatic expression of Bambi mRNA also was significantly lower in the HC diet group than in the control group (Supplementary Figure 6).

Third, the effect of FC on the HSC sensitivity to TGFβ was evaluated. Niemann-Pick C1 (NPC1) is a late endosomal protein that regulates intracellular cholesterol transport. Homozygous NPC1-deficient cells have been shown to accumulate intracellular FC.[9,10] Therefore, HSCs isolated from NPC1 knock-out (KO) mice were used for analysis. Before treatment with TGFβ, no significant differences were found between WT and NPC1 KO HSCs in the expression levels of collagen 1α1, collagen 1α2, or αSMA mRNA transcripts. Treatment with TGFβ significantly increased the levels of collagen 1α1, collagen 1α2, and αSMA mRNA transcripts. The positive effect was seen more markedly in NPC1 KO HSCs than in WT HSCs (Figure 5*C*, *left three panels*). Bambi mRNA levels were

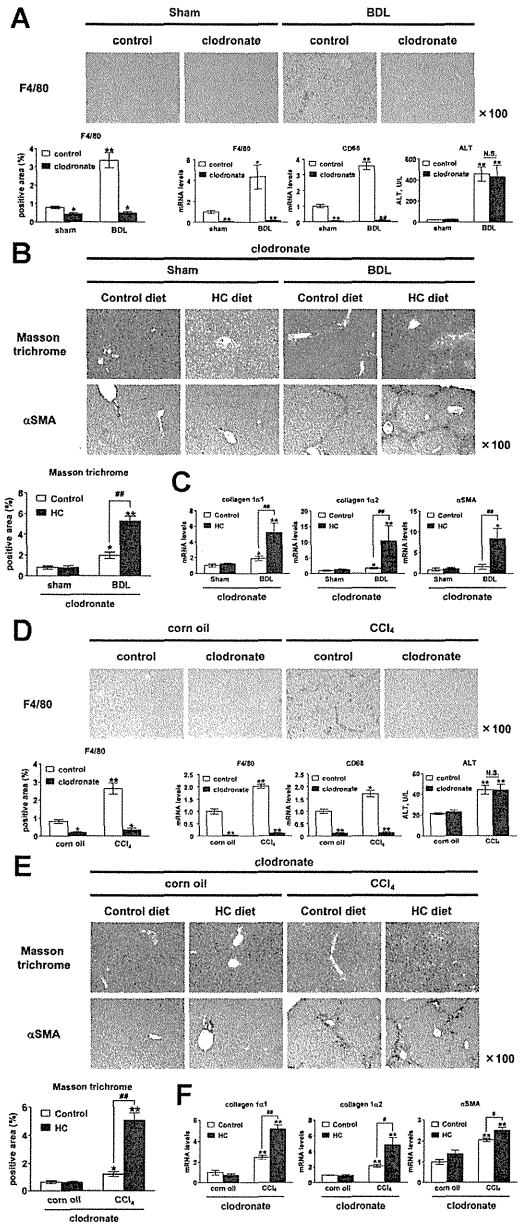

Figure 4. Depletion of Kupffer cells does not abrogate the effects of the HC diet on hepatic fibrosis induced by BDL or CCl_4 treatment. WT C57BL/6 mice were injected with liposomal clodronate or vehicle. Thereafter, animals were subjected to (*A–C*) BDL or (*D–F*) CCl_4 intoxication to induce liver fibrosis. (*A* and *D*, *upper panels*) Immunohistochemical staining for F4/80. (*A* and *D*, *lower panels*) Quantification of immunohistochemical staining for F4/80 (*left*). Hepatic expression of F4/80 and CD68 mRNA (N = 4–7/group) (*middle*), and serum ALT levels (*right*). *$P < .05$ and **$P < .01$ compared with the (*A*) vehicle-treated–sham-operated group or the (*D*) vehicle-treated–corn oil group. (*B* and *E*, *upper panels*) Masson trichrome staining. (*B* and *E*, *middle panels*) Immunohistochemical detection of αSMA. (*B* and *E*, *lower panels*) Quantification of Masson trichrome staining. (C and *F*) Hepatic expression of collagen 1α1, collagen 1α2, and αSMA mRNA (N = 4–7/group). *$P < .05$ and **$P < .01$ compared with the (*B* and *C*) control diet–sham-operated group or the (*E* and *F*) control diet–corn oil group. #$P < .05$ and ##$P < .01$ compared with the (*B* and *C*) control diet–BDL group or the (*E* and *F*) control diet–CCl_4 group.

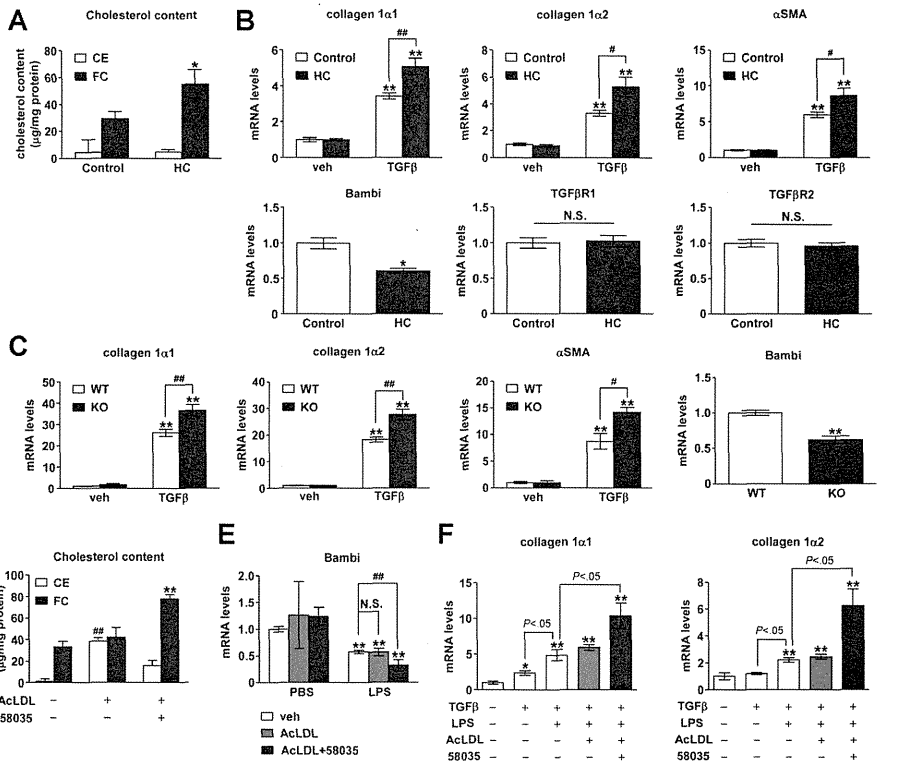

Figure 5. FC, but not CE, promotes TGFβ-induced HSC activation. (*A*) Quantification of cellular FC and CE in HSCs immediately after isolation from control diet–fed or HC diet–fed mice (N = 5–7/group). *$P < .05$ vs control-diet group. (*B*) Expression of (*upper panels*) collagen 1α1, collagen 1α2, αSMA, and (*lower panels*) Bambi, TGFβR1, and TGFβ R2 mRNA in primary HSC cultures. (*Upper panels*) Primary HSCs isolated from control diet–fed or HC diet–fed mice were treated or not treated with TGFβ (1 ng/mL) for 6 hours. (*Lower panels*) HSCs separated from control diet–fed or HC diet–fed mice were analyzed with real-time polymerase chain reaction (N = 5–7/group). *$P < .05$ and **$P < .01$ vs the control diet–control culture. #$P < 0.05$ and ##$P < 0.01$ vs the control diet–TGFβ-treated culture. (*C*) Expression of (*left three panels*) collagen 1α1, collagen 1α2, αSMA, and (*far right panel*) Bambi mRNA in primary HSC cultures. (*Left three panels*) Primary HSCs isolated from WT mice or NPC1-deficient mice were treated with TGFβ (1 ng/mL) or not for 6 hours. (*Far right panel*) HSCs separated from WT mice or NPC1-deficient mice were analyzed by real-time polymerase chain reaction (N = 5–7/group). **$P < 0.01$ vs the WT mice–control culture. #$P < .05$ and ##$P < .01$ vs the WT mice–TGFβ-treated culture. (*D*) Quantification of cellular FC and CE in primary cultured HSCs. HSCs were incubated with vehicle, AcLDL (50 μg/mL), or AcLDL plus compound 58035 (10 μg/mL) for 16 hours (N = 5–7/group). **$P < .01$ vs cellular FC content in the vehicle-treated culture. ##$P < .01$ vs cellular CE content in the vehicle-treated culture. (*E*) Expression of Bambi mRNA in primary HSC cultures. HSCs were incubated with vehicle, AcLDL, or AcLDL plus compound 58035 for 16 hours, and then treated with LPS (100 ng/mL) or not for 6 hours (N = 5–7/group). **$P < .01$ vs the corresponding culture without LPS treatment in each group. ##$P < .01$ vs the LPS-treated control culture. (*F*) Expression of collagen 1α1 and collagen 1α2 mRNA in primary HSC cultures. HSCs were incubated with vehicle, AcLDL, or AcLDL plus compound 58035 for 16 hours, and then treated with LPS (100 ng/mL) or not for 6 hours, before the addition of TGFβ for an additional 6 hours (N = 5–7/group). *$P < .05$ and **$P < .01$ vs the vehicle-treated control culture.

significantly lower in NPC1 KO HSCs relative to WT HSCs (Figure 5*C*, *far right panel*). It has been reported that cholesterol accumulates predominantly in late endosomes/lysosomes of cells in NPC1 KO mice.[9] Our study also found that FC levels in late endosomes/lysosomes were significantly higher in NPC1 KO HSCs than in WT HSCs (Supplementary Figure 7*A*). Similarly, FC levels in late endosomes/lysosomes were significantly higher in the HSCs from the HC diet group than in those from the control diet group (Supplementary Figure 7*B*).

It has been reported that FC accumulates in cells treated with the combination of acetyl low-density lipoprotein (AcLDL) and acyl-CoA:cholesterol acyltransferase inhibitor 58035 (compound 58035), whereas CE accumulates in cells

BASIC AND TRANSLATIONAL LIVER

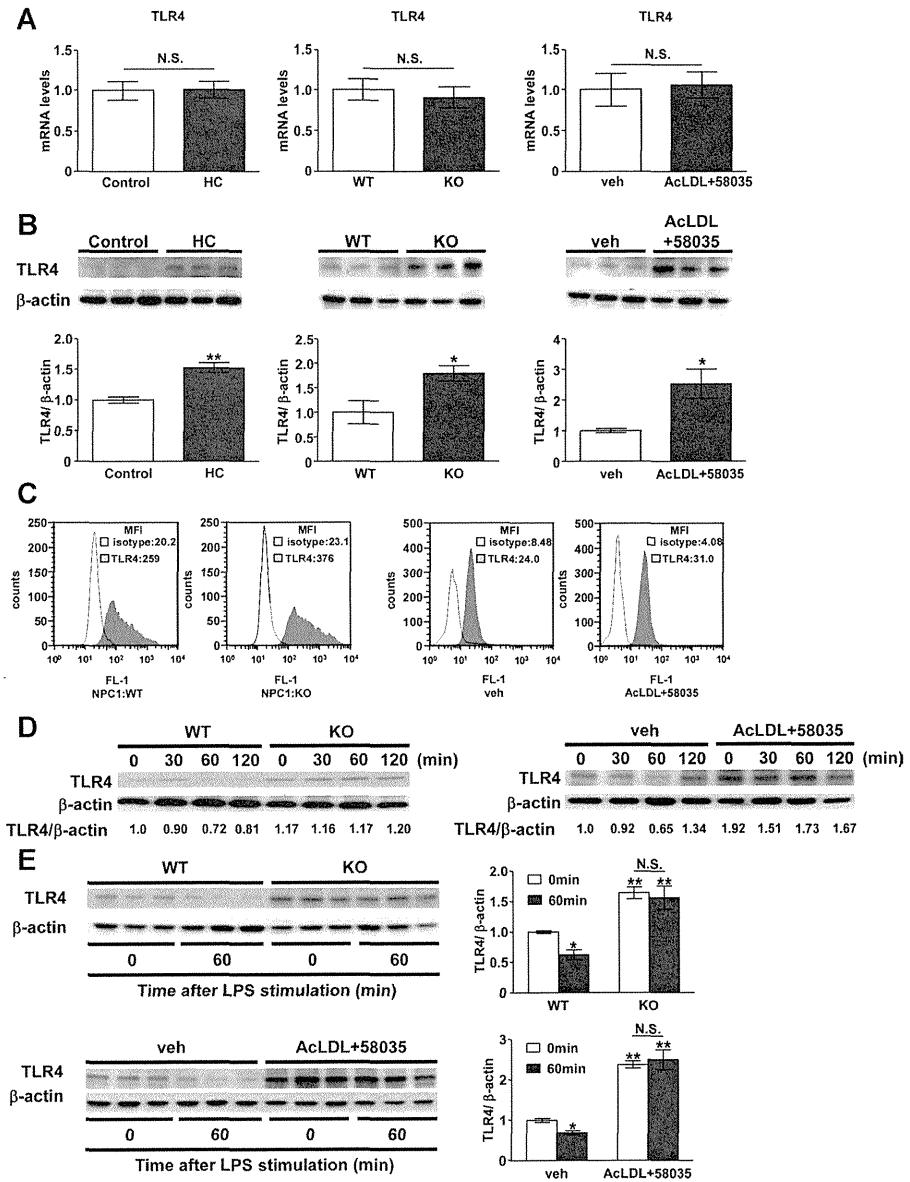

treated with AcLDL alone.[11] In our study, treatment of HSCs with AcLDL plus compound 58035 significantly increased FC accumulation, and treatment with AcLDL alone significantly promoted CE accumulation (Figure 5*D*). However, the Bambi expression levels were not decreased when HSCs were treated with either AcLDL alone or the combination of AcLDL and compound 58035 (Figure 5*E*). The expression of the Bambi gene in HSCs has been reported to depend on TLR4 signaling and decreases with the addition of lipopolysaccharide (LPS).[12] In our study as well, Bambi mRNA expression levels were decreased significantly when HSCs were treated with LPS (Figure 5*E*). The decrease in Bambi mRNA levels was enhanced significantly when cells were treated with AcLDL plus compound 58035, whereas cells treated with AcLDL alone did not show a significant reduction compared with controls (Figure 5*E*). The accumulation of FC in HSCs also intensified LPS-mediated TLR4 signal transduction to induce proinflammatory cytokines such as monocyte chemoattractant protein-1 and macrophage inflammatory protein-2 (Supplementary Figures 8*A* and *B*), which are known to be up-regulated by the LPS-mediated TLR4 signal pathway in HSCs.[12,13] HSCs pretreated with LPS showed a significant enhancement of collagen 1α1 and 1α2 mRNA expression when stimulated with TGFβ (Figure 5*F*). These cells showed a further increase in the mRNA expression of these genes when loaded with AcLDL plus compound 58035, whereas no significant increase was observed when cells were incubated with AcLDL alone (Figure 5*F*). These results clearly indicate that FC accumulation in HSCs sensitized them to TGFβ-induced signals by down-regulating Bambi gene expression.

Unlike HSCs, there were no significant differences in Kupffer cell FC levels between the HC diet group and the control diet group; however, CE levels were significantly higher in Kupffer cells from the HC diet group than in those from the control diet group (Supplementary Figure 9*A*). An accumulation of CE did not accelerate TNFα mRNA expression in Kupffer cells (Supplementary Figure 9*B*), nor did it enhance LPS-induced TNFα mRNA expression in these cells (Supplementary Figure 9*B*). These results show that the HC diet did not cause Kupffer cells to trigger hepatic fibrosis, although it did increase Kupffer cell CE levels.

Accumulation of FC in HSCs Up-Regulated TLR4 Expression

Consumption of the HC diet did not affect TLR4 mRNA expression levels in HSCs. However, the HC diet increased the amount of TLR4 protein expressed in HSCs (Figure 6*A* and *B*). In addition, increased levels of TLR4 gene expression in terms of the amount of protein (but not mRNA) also were observed in NPC1 KO HSCs and HSCs stimulated with AcLDL plus compound 58035 (Figure 6*A* and *B*). Moreover, NPC1 KO HSCs showed higher TLR4 protein membrane expression relative to WT HSCs (Figure 6*C*). Similar results were obtained for HSCs treated with AcLDL plus compound 58035 (Figure 6*C*).

Under normal conditions, membrane proteins are internalized into the cytoplasm by endocytosis, where they are degraded by endosomal–lysosomal or proteasomal pathways. Ligand formation enhances the endocytotic activity, and, consequently, degradation of membrane proteins is accelerated.[14] To investigate the role of FC in TLR4 expression, we examined the dynamic change in the quantity of TLR4 protein in cells treated with LPS. We found that TLR4 protein expression was decreased 60 minutes after LPS treatments in WT HSCs, whereas that in NPC1 KO HSCs remained at a high level after LPS treatments (Figure 6*D*, *left row*, and *E*, *top row*). Similar results were obtained for HSCs treated with AcLDL plus compound 58035 (Figure 6*D*, *right row*, and *E*, *bottom row*). These results clearly show that HSC accumulation of FC significantly increased TLR4 protein content. We conjectured that intercellular FC accumulation probably suppressed the ligand-mediated enhanced degradation of TLR4.

HC Diet-Induced Aggravation of Liver Fibrosis Was Dependent on TLR4 Signal Transduction in HSCs

In the last part of the experiment, we used LPS-unresponsive C3H/HeJ mice (TLR4 mutant) to assess whether HC diet-induced aggravation of liver fibrosis was dependent on TLR4 signal transduction. Unlike the results obtained with WT mice, HC diet consumption did not enhance the progression of BDL-induced liver fibrosis in C3H/HeJ mice (Figure 7*A* and *B*). Similarly, the HC diet did not hasten the progression of CCl_4-induced liver fibrosis (Figure 7*C* and *D*).

Next, we examined whether HSC activation by accumulated FC required TLR4 signaling in HSCs. Samples of HSCs were collected from C3H/HeJ mice given the control or HC diet for 4 weeks, and used for study. Treatment with TGFβ significantly enhanced the levels of collagen 1α1, collagen 1α2, and αSMA mRNA transcripts in HSCs. However, unlike the results obtained with WT mouse HSCs, no significant difference was found between the HC and control diet

Figure 6. FC enhances protein expression of TLR4 in HSCs. TLR4 (*A*) mRNA and (*B*) protein expression (HSCs isolated from control diet-fed or HC-fed mice [*left*], WT or NPC1-deficient HSCs [*middle*], vehicle-treated or FC-loaded HSCs [*right*]). (*B*, *lower panels*) Quantification of TLR4 protein expression. $^{**}P < .01$ vs control-diet group (*left*); $^{*}P < .05$ vs WT HSCs (*middle*); and $^{*}P < .05$ vs vehicle-treated HSCs (*right*). (*C*) Fluorescence-activated cell sorter assay of TLR4 expression on plasma membranes of WT or NPC1-deficient HSCs (*left*) and vehicle-treated or FC-loaded HSCs (*right*). The mean fluorescence intensity (MFI) is also shown at the upper right corner of each panel. (*D*) Dynamic changes and (*E*) quantification of TLR4 protein expression in WT or NPC1-deficient HSCs (*D*, *left panels*; *E*, *upper panels*), and vehicle-treated or FC-loaded HSCs (*D*, *right panels*; *E*, *lower panels*) shown at the time after LPS (100 ng/mL) treatment. The relative levels of TLR4 to β-actin are indicated below the corresponding bands. $^{*}P < .05$ and $^{**}P < .01$ vs the WT HSCs or vehicle-treated HSCs before LPS treatment. HSCs cultured 6 days after isolation from mice or rats were used (*C*–*E*).

BASIC AND TRANSLATIONAL LIVER

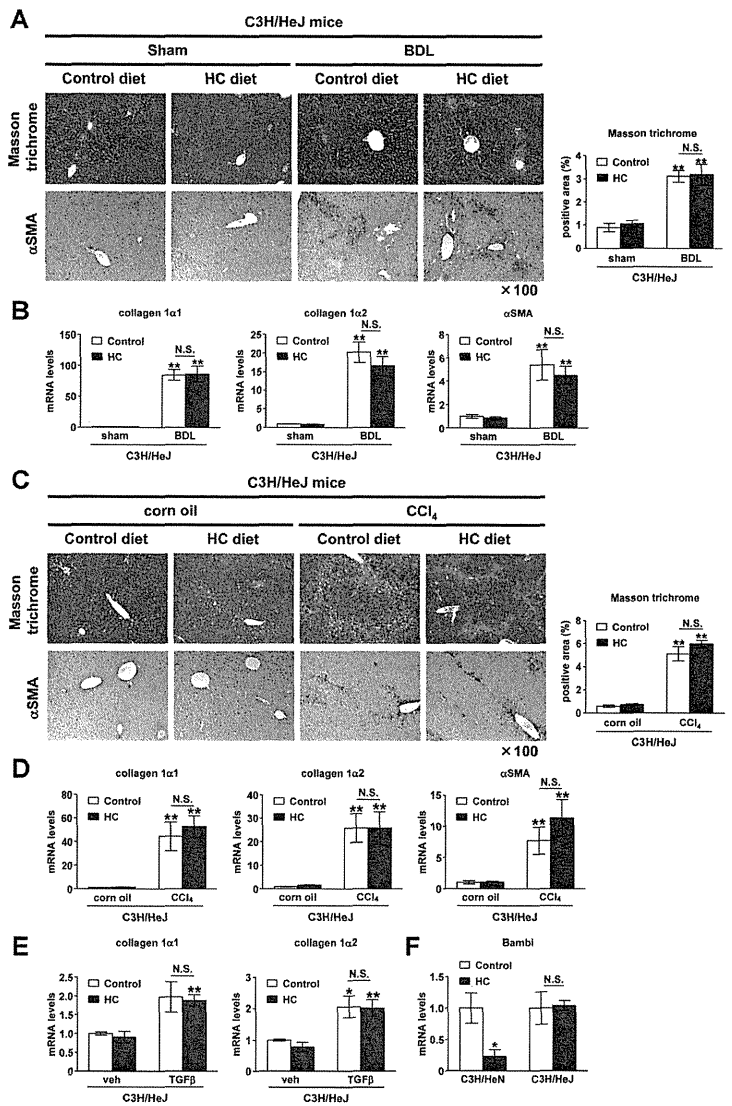

Figure 7. HC diet–induced aggravation of liver fibrosis was dependent on TLR4 signal transduction in HSCs. TLR4 mutant (C3H/HeJ) mice were fed a control or HC diet for 4 weeks. Then, while remaining on the same diet, animals were subjected to (*A* and *B*) BDL or (*C* and *D*) CCl_4 intoxication for induction of liver fibrosis (N = 4–7/group). (*A* and *C*) Masson trichrome staining (*left upper panels*) and immunohistochemical staining for α-SMA (*left lower panels*). Quantification of Masson trichrome staining (*right panels*). (*B* and *D*) Hepatic expression of collagen 1α1, collagen 1α2, and αSMA mRNA (N = 4–7/group). $^{**}P < .01$ compared with the (*B*) control diet–sham-operated group or the (*D*) control diet–corn oil group. (*E*) Expression of collagen 1α1 and collagen 1α2 mRNA in primary HSCs. HSCs isolated from control diet–fed or HC diet–fed C3H/HeJ mice were treated or not treated with TGFβ (1 ng/mL) for 6 hours (N = 5–7/group). $^{*}P < .05$ and $^{**}P < .01$ vs the control diet–control culture. (*F*) Expression of Bambi mRNA in primary HSCs isolated from C3H/HeN mice or C3H/HeJ mice, fed a control or an HC diet (N = 5–7/group). $^{*}P < .05$ vs the control diet–C3H/HeN mice group.

groups (Figure 7*E*). Moreover, although HC diet consumption significantly attenuated Bambi gene expression in HSCs isolated from C3H/HeN mice (WT control for C3H/HeJ mice), the HSC Bambi mRNA level was not affected in C3H/HeJ mice (Figure 7*F*).

These findings clearly show that HC diet-induced aggravation of liver fibrosis was dependent on TLR4 signal transduction. Our study suggested that HC diet consumption attenuated HSC Bambi expression via TLR4 signaling, which led to the aggravation of BDL- or CCl_4-induced liver fibrosis.

Discussion

Our present results clearly show that an HC diet aggravated BDL- and CCl_4-induced liver fibrosis, although an HC diet alone was not sufficient for inducing liver fibrosis. TGFβ, the most potent factor predisposing to human fibrogenesis, has been shown to play a central role in the pathophysiology of liver fibrosis.[1] Moreover, these results showed that major causes for exacerbation of liver fibrosis involved HSC accumulation of cholesterol in the form of FC, which sensitized HSCs to TGFβ-induced activation.

Recent research has shown that intracellular FC accumulation increased TLR4 protein levels in the membrane fraction to facilitate TLR4 signaling activation.[15] Our results showed that HSC accumulation of FC increased cytomembrane-bound TLR4 protein levels; however, the amounts of TLR4 mRNA transcripts were similar. Under normal conditions, cytomembrane TLR4 protein molecules are transferred into the cytoplasm by endocytosis, and degraded by endosomal–lysosomal or proteasomal pathways. Degradation of cytomembrane TLR4 proteins is accelerated when internalization of these molecules is promoted by ligand formation. Inhibition of the degradation pathways intensifies ligand-mediated TLR4 signal transduction.[14] In our study, the level of the TLR4 protein in HSCs was lowered significantly in cells incubated with LPS, the major ligand for TLR4. Moreover, the LPS-induced decrease in the HSC level of the TLR4 protein was inhibited prominently by FC accumulated in HSCs. These results suggest that FC accumulated in HSCs inhibited the TLR4 degradation pathway, thereby increasing TLR4 protein levels.

In the present study, FC levels in late endosomes/lysosomes were significantly higher in HSCs from the HC diet group or NPC1 KO mice than in those from the control diet group or WT mice. Recent studies have reported that FC modulated the endosomal–lysosomal pathway of endocytosis through regulation of endosome motility.[16] NPC1 KO mice, which accumulate intracellular FC predominantly in late endosomes/lysosomes, were found to retain amyloid precursor proteins as a result of endosomal dysfunction.[9] NPC1 KO mice also were found to show autophagic–lysosomal dysfunction in the brain.[10] These findings suggest that FC accumulation in HSCs is involved in endosomal–lysosomal dysfunction, leading to TLR4 protein accumulation.

The expression of the TGFβ pseudoreceptor Bambi in HSCs was solely dependent on TLR4 signaling.[12] The activation of TLR4 signaling in HSCs, which down-regulates the expression of the downstream Bambi gene, was reported to sensitize HSCs to TGFβ-induced activation, contributing to advancement of liver fibrosis.[12] In our study, HSCs also showed a significantly decreased expression of the Bambi gene when incubated with the TLR4 ligand LPS. The HSC accumulation of FC (not CE) significantly promoted LPS-mediated Bambi down-regulation and markedly accelerated (LPS-mediated) enhancement of HSC sensitivity against TGFβ signaling. We contend that these changes activated HSCs further, thereby promoting liver fibrosis.

In our experiment, TLR4-mutant C3H/HeJ mice given the HC diet did not show aggravation of liver fibrosis. Accumulation of FC in HSCs collected from TLR4-mutant mice did not give rise to Bambi down-regulation, and no change was observed in the HSC sensitivity against TGFβ signaling. Based on these results, we concluded that the activation of the TLR4 signal pathway mediated by FC accumulated in HSCs played a critical role in HC diet-induced exacerbation of liver fibrosis.

In the murine liver fibrosis models reported here, consumption of an HC diet neither affected hepatocyte injury nor influenced the pathophysiology of liver inflammation, including Kupffer cell activation.

Marí et al[17] found that FC accumulated in hepatocytes exacerbated LPS-mediated acute liver injury in a manner that induced susceptibility of hepatocytes to TNFα-mediated apoptosis. However, several other researchers claimed that TNFα-mediated hepatocyte apoptosis was not involved in the progression of liver fibrosis,[18,19] and their findings seem to shed light on the reason why cholesterol accumulation in hepatocytes resulting from consumption of an HC diet did not significantly exacerbate hepatocyte damage, as shown in our study. Wouters et al[20] reported that administration of a high-fat HC diet in low-density lipoprotein receptor KO and apolipoprotein E KO mice caused liver inflammation and the transformation of Kupffer cells into foam cells. However, HC diet consumption did not trigger macrophage foam cell formation in the models used in our study. We also clearly showed that an HC diet aggravated BDL- and CCl_4-induced liver fibrosis in mice depleted of Kupffer cells by administration of clodronate. Altogether, these results suggest that HSCs, rather than hepatocytes or Kupffer cells, should be focused on as the primary site of alterations in liver fibrosis resulting from HC diet consumption.

In summary, our study has provided new insights into the mechanisms linking HC diet uptake and liver fibrosis. The HC diet-induced accumulation of FC in HSCs promoted TLR4 signal transduction by increasing membrane TLR4 levels, and thereby suppressed the HSC expression of the Bambi gene. Consequently, HSC TGFβ signaling was boosted, resulting in HSC activation and progression of liver fibrosis.

Our present work indicates that in the process of liver fibrosis progression, cholesterol functions as a signal-enhancing factor FC that accumulates in HSCs, rather than as an extracellular activation-inducible factor for HSCs. The findings of this study warrant further investigations that focus on FC in HSCs as the target of new therapeutic strategies for the treatment of liver fibrosis.

Supplementary Material

Note: To access the supplementary material accompanying this article, visit the online version of

BASIC AND TRANSLATIONAL LIVER

Gastroenterology at www.gastrojournal.org, and at doi: 10.1053/j.gastro.

References

1. Friedman SL. Mechanisms of hepatic fibrogenesis. Gastroenterology 2008;134:1655–1669.
2. Ioannou GN, Morrow OB, Connole ML, et al. Association between dietary nutrient composition and the incidence of cirrhosis or liver cancer in the United States population. Hepatology 2009;50: 175–184.
3. Ekstedt M, Franzén LE, Mathiesen UL, et al. Statins in non-alcoholic fatty liver disease and chronically elevated liver enzymes: a histopathological follow-up study. J Hepatol 2007;47: 135–141.
4. Yoneda M, Fujita K, Nozaki Y, et al. Efficacy of ezetimibe for the treatment of non-alcoholic steatohepatitis: an open-label, pilot study. Hepatol Res 2010;40:613–621.
5. Sumiyoshi M, Sakanaka M, Kimura Y. Chronic intake of a high-cholesterol diet resulted in hepatic steatosis, focal nodular hyperplasia and fibrosis in non-obese mice. Br J Nutr 2010;103:378–385.
6. Kainuma M, Fujimoto M, Sekiya N, et al. Cholesterol-fed rabbit as a unique model of nonalcoholic, nonobese, non-insulin-resistant fatty liver disease with characteristic fibrosis. J Gastroenterol 2006;41:971–980.
7. Vergnes L, Phan J, Strauss M, et al. Cholesterol and cholate components of an atherogenic diet induce distinct stages of hepatic inflammatory gene expression. J Biol Chem 2003;278: 42774–42784.
8. Malhi H, Bronk SF, Werneburg NW, et al. Free fatty acids induce JNK-dependent hepatocyte lipoapoptosis. J Biol Chem 2006;281: 12093–12101.
9. Jin LW, Shie FS, Maezawa I, et al. Intracellular accumulation of amyloidogenic fragments of amyloid-beta precursor protein in neurons with Niemann-Pick type C defects is associated with endosomal abnormalities. Am J Pathol 2004;164:975–985.
10. Liao G, Yao Y, Liu J, et al. Cholesterol accumulation is associated with lysosomal dysfunction and autophagic stress in Npc1 −/− mouse brain. Am J Pathol 2007;171:962–975.
11. Li Y, Schwabe RF, DeVries-Seimon T, et al. Free cholesterol-loaded macrophages are an abundant source of tumor necrosis factor-alpha and interleukin-6: model of NF-kappaB- and map kinase-dependent inflammation in advanced atherosclerosis. J Biol Chem 2005;280:21763–21772.
12. Seki E, De Minicis S, Osterreicher CH, et al. TLR4 enhances TGF-beta signaling and hepatic fibrosis. Nat Med 2007;13:1324–1332.
13. Paik YH, Schwabe RF, Bataller R, et al. Toll-like receptor 4 mediates inflammatory signaling by bacterial lipopolysaccharide in human hepatic stellate cells. Hepatology 2003;37:1043–1055.
14. Wang Y, Chen T, Han C, et al. Lysosome-associated small Rab GTPase Rab7b negatively regulates TLR4 signaling in macrophages by promoting lysosomal degradation of TLR4. Blood 2007;110:962–971.
15. Suzuki M, Sugimoto Y, Ohsaki Y, et al. Endosomal accumulation of Toll-like receptor 4 causes constitutive secretion of cytokines and activation of signal transducers and activators of transcription in Niemann-Pick disease type C (NPC) fibroblasts: a potential basis for glial cell activation in the NPC brain. J Neurosci 2007; 27:1879–1891.
16. Chen H, Yang J, Low PS, et al. Cholesterol level regulates endosome motility via Rab proteins. Biophys J 2008;94:1508–1520.
17. Marí M, Caballero F, Colell A, et al. Mitochondrial free cholesterol loading sensitizes to TNF- and Fas-mediated steatohepatitis. Cell Metab 2006;4:185–198.
18. Bohan A, Chen WS, Denson LA, et al. Tumor necrosis factor alpha-dependent up-regulation of Lrh-1 and Mrp3(Abcc3) reduces liver injury in obstructive cholestasis. J Biol Chem 2003;278: 36688–36698.
19. Simeonova PP, Gallucci RM, Hulderman T, et al. The role of tumor necrosis factor-alpha in liver toxicity, inflammation, and fibrosis induced by carbon tetrachloride. Toxicol Appl Pharmacol 2001; 177:112–120.
20. Wouters K, van Gorp PJ, Bieghs V, et al. Dietary cholesterol, rather than liver steatosis, leads to hepatic inflammation in hyperlipidemic mouse models of nonalcoholic steatohepatitis. Hepatology 2008;48:474–486.

Received November 13, 2010. Accepted September 24, 2011.

Reprint requests

Address requests for reprints to: Kengo Tomita, MD, PhD, Division of Gastroenterology and Hepatology, Department of Internal Medicine, National Defense Medical College, 3-2 Namiki, Tokorozawa-shi, Saitama 359-8513, Japan. e-mail: kengo@ndmc.ac.jp; fax: (81) 4-2996-5201.

Acknowledgments

The authors thank Mina Kitazume and Miho Takabe (Keio University) for helpful advice and technical assistance; and Drs Shuhji Seki, Manabu Kinoshita, and Hiroyuki Nakashima (Department of Immunology and Microbiology, National Defense Medical College) for helpful discussion and critical comments.

T. Teratani and K. Tomita contributed equally to this work and share first authorship.

Conflicts of interest

The authors disclose no conflicts.

Funding

This study was supported in part by a Grant-in-Aid for Scientific Research from the Ministry of Education, Culture, Sports, Science, and Technology of Japan (to K. Tomita).

Supplementary Materials and Methods

Reagents

Reagents were obtained as follows: AcLDL was from Biomedical Technologies (Stoughton, MA). Compound 58035 and LPS were from Sigma (St. Louis, MO). TGFβ was from R&D Systems (Minneapolis, MN). CCl_4 was from Wako Pure Chemical Industries (Osaka, Japan).

Animal Model

Male WT C57BL/6, C3H/HeN, and C3H/HeJ mice and Sprague–Dawley rats were purchased from Sankyo Laboratories (Tokyo, Japan). $NPC1^{-/-}$ mice were purchased from Jackson Laboratories (Bar Harbor, ME). Mice were bred and housed in a temperature- and light-controlled facility with unlimited access to food and water. For BDL, we anesthetized mice and after midline laparotomy we ligated the common bile duct twice with silk sutures and closed the abdomen. We performed the sham surgery similarly, except that the bile duct was not ligated. Mice were killed 3 weeks after BDL. For acute liver injury, mice were fed a control or an HC diet for 4 weeks, and then were killed 5 days after BDL or 24 hours after a single injection of CCl_4. All animals received humane care in compliance with the National Research Council's criteria outlined in the "Guide for the Care and Use of Laboratory Animals," prepared by the US National Academy of Sciences and published by the US National Institutes of Health (Bethesda, MD).

Biochemical and Histologic Analysis

Serum concentrations of ALT, TGs, glucose, and cholesterol were determined as previously described. Hepatic TG content and liver hydroxyproline concentrations were measured as previously described.[1] Liver cholesterol levels or the cholesterol content of HSCs or Kupffer cells were measured using the Cholesterol/Cholesteryl Ester Quantitation Kit (BioVision, Mountain View, CA), following the manufacturer's instructions. We detemined the cholesterol content of HSCs or Kupffer cells immediately after isolation. Liver tissues were fixed in 4% paraformaldehyde, embedded in paraffin, and stained with H&E and a Masson trichrome solution. For protein or RNA analysis, tissues were frozen in liquid nitrogen and stored at −80°C until needed.

Kupffer Cell Depletion

We injected dichloromethylene diphosphonic acid (clodronate)-loaded or phosphate-buffered saline–loaded liposomes (Encapsula NanoSciences, Nashville, TN) intravenously into mice (200 μL per mouse).

HSC Isolation and Culture

HSCs were isolated from mice or rats as previously described.[1] We cultured HSCs on uncoated plastic tissue culture dishes in Dulbecco's modified Eagle medium containing 1% or 10% fetal bovine serum, and used them as nonpassaged primary cultures only. For FC accmulation in HSCs, primary HSCs were incubated with AcLDL (50 μg/mL) plus compound 58035 (10 μg/mL) for 16 hours. We used enzyme-linked immunosorbent assay kits for mouse monocyte chemoattractant protein-1 (Thermo Scientific, Rodkford, IL) or macrophage inflammatory protein-2 (R&D Systems) for quantification of secreted monocyte chemoattractant protein-1 and macrophage inflammatory protein-2 in HSC cultures.

Kupffer Cell Isolation and Culture

Kupffer cells were isolated from mice, and cultured as previously described.[2]

Immunohistochemistry

Paraffinized sections were deparaffinized, rehydrated, blocked with normal horse serum, and incubated with anti-αSMA monoclonal antibody 1A4 (Dako Japan, Kyoto, Japan), anti-F4/80 monoclonal antibody (Serotec, Oxford, UK), or anti-CD3 monoclonal antibody (Abcam, Cambridge, UK) overnight at 4°C. The mouse F4/80 antigen is a 160-kilodalton glycoprotein expressed by mouse macrophages; antimouse F4/80 antibody binds mouse monocytes/macrophages and Kupffer cells. The antigen is not expressed by either lymphocytes or polymorphonuclear cells. Antibody binding was detected by incubation with biotinylated antimouse immunoglobulin G antibody and visualized with a Vectastain Elite ABC Kit (Vector Laboratories, Inc, Burlingame, CA) by reaction with Vectastatin DAB Substrate (Vector).

Fresh-frozen liver sections were cut 6-mm thick on a cryostat, collected on slides, and immediately dried. The sections were fixed with acetone. The slides were incubated overnight with anti-CD68 Ab (Serotec), followed by incubation with Histofine Simple Stain Mouse MAX-PO (Nichirei, Tokyo, Japan) for 1 hour.

Neutrophil Infiltration

Neutrophils in the liver were stained using the naphthol AS-D chloroacetate esterase technique. Paraffin-embedded liver sections were stained using the naphthol AS-D chloroacetate kit (Sigma Chemical Co, St. Louis, MO) following the manufacturer's instructions.

Detection of Apoptosis

Terminal deoxynucleotidyl transferase–mediated deoxyuridine nick-end labeling staining (Chemicon International, Temecula, CA) was performed on specimens to assess apoptosis. Apoptosis was quantified by counting positively stained cells in 10 random fields at 200× magnification. Apoptosis was measured for each specimen as a percentage of total cells per field. Antibody binding was detected by incubation with biotinylated anti-mouse immunoglobulin G antibody and visualized with a Vectastain Elite ABC Kit (Vector Laboratories, Inc) by reaction with Vectastatin DAB Substrate (Vector).

Mitochondrial Isolation and Characterization

A mitochondrial fraction was enriched from 100-mg liver specimens with the Mitochondria Isolation Kit (Sigma) by 2 consecutive centrifugation steps at 600 g and 11,000 g. The electrochemical proton gradient ($\Delta\Psi$) of the inner mitochondrial membrane was tested by measuring the uptake of the fluorescent carbocyanine dye JC-1 (Sigma) into mitochondria, as specified by the manufacturer.[1] Relative $\Delta\Psi$ was calculated in comparison with values obtained in control-diet–fed mice.

Real-Time Quantitative and Reverse-Transcription Polymerase Chain Reaction Analysis

Total RNA was extracted from total liver homogenates or HSCs using TaKaRa RNAiso Reagent (TaKaRa Bio, Ohtsu, Japan), according to the manufacturer's instructions. Reverse transcription was performed as previously described.[1] For quantitation of mRNA expression, the following real-time polymerase chain reaction amplifications were performed in duplicate, using the SYBR Premix Ex Taq (Perfect Real Time) kit (TaKaRa Bio) in a Thermal Cycler Dice Real Time system (TaKaRa Bio).

Western Blot Analysis

Preparation of whole-cell protein extracts from HSCs, electrophoresis of whole-cell protein extracts (5 μg), and subsequent blotting were performed using antibodies against TLR4 and β-actin, as previously described.[1]

Flow Cytometry Analysis

HSC surface expression of TLR4 was detected by flow cytometry of live cells stained with phycoerythrin-conjugated anti-TLR4 antibody (Abcam) or phycoerythrin-conjugated anti-immunoglobulin G isotype control. A total of 10,000 cells/condition were analyzed in a FACScan, using the FACSCalibur (Becton Dickinson, Franklin Lakes, NJ).

Isolation of Late Endosomes/Lysosomes From HSCs

Late endosomal/lysosomal fractions were prepared from HSCs using the lysosome isolation kit (Sigma) following the manufacturer's instructions.

References

1. Tomita K, Tamiya G, Ando S, et al. Tumour necrosis factor alpha signalling through activation of Kupffer cells plays an essential role in liver fibrosis of non-alcoholic steatohepatitis in mice. Gut 2006; 55:415–424.
2. Tomita K, Azuma T, Kitamura N, et al. Leptin deficiency enhances sensitivity of rats to alcoholic steatohepatitis through suppression of metallothionein. Am J Physiol Gastrointest Liver Physiol 2004; 284:G1078–G1085.
3. Paik YH, Schwabe RF, Bataller R, et al. Toll-like receptor 4 mediates inflammatory signaling by bacterial lipopolysaccharide in human hepatic stellate cells. Hepatology 2003;37:1043–1055.
4. Seki E, De Minicis S, Osterreicher CH, et al. TLR4 enhances TGF-beta signaling and hepatic fibrosis. Nat Med 2007;13:1324–1332.

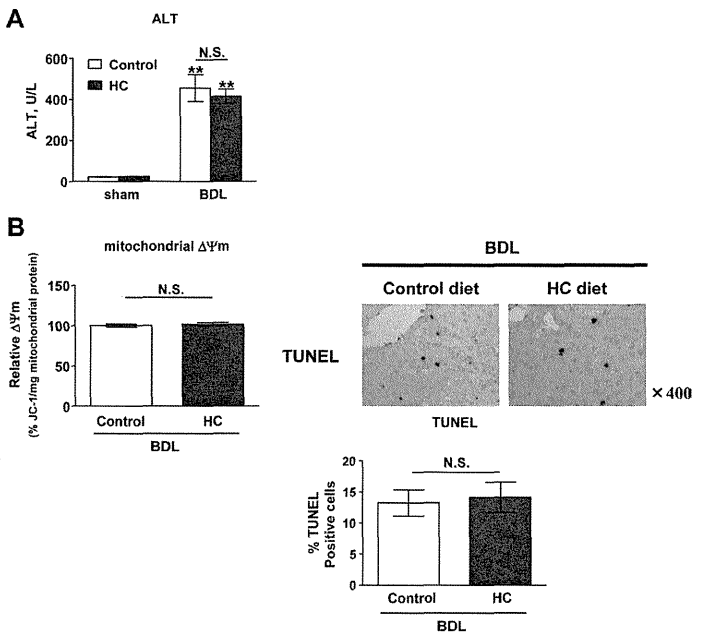

Supplementary Figure 1. Effects of the HC diet on acute liver injury induced by BDL treatment. After being fed a control or an HC diet for 4 weeks, C57BL/6 mice were subjected to acute liver injury, induced 5 days after BDL treatment (N = 5/group). (*A*) Serum ALT activities (N = 5/group). (*B, left panels*) Electrochemical proton gradient of the inner mitochondrial membrane (N = 5/group). The calculated relative $\Delta\Psi$ was normalized to the values obtained in mice from the control diet–BDL group. (*B, right panels*) The percentage of terminal deoxynucleotidyl transferase–mediated deoxyuridine nick-end labeling (TUNEL)-positive hepatocytes (N = 5/group) and the representative sections.

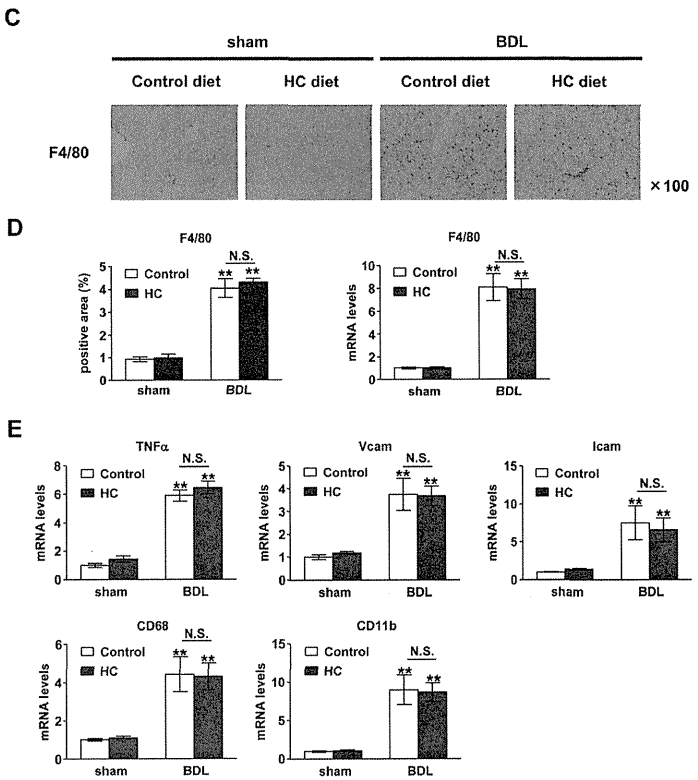

Supplementary Figure 1 (Cont'd.). (*C*) Immunohistochemical detection of F4/80-positive cells in livers. (*D*) Quantification of F4/80 by immunohistochemical staining and mRNA levels. (*E*) Hepatic expression of TNFα, vascular cell adhesion molecule-1 (VCAM-1), intercellular adhesion molecule-1 (ICAM-1), CD68, and CD11b mRNA (N = 5/group). $^{**}P < .01$ compared with control diet–sham-operated group.

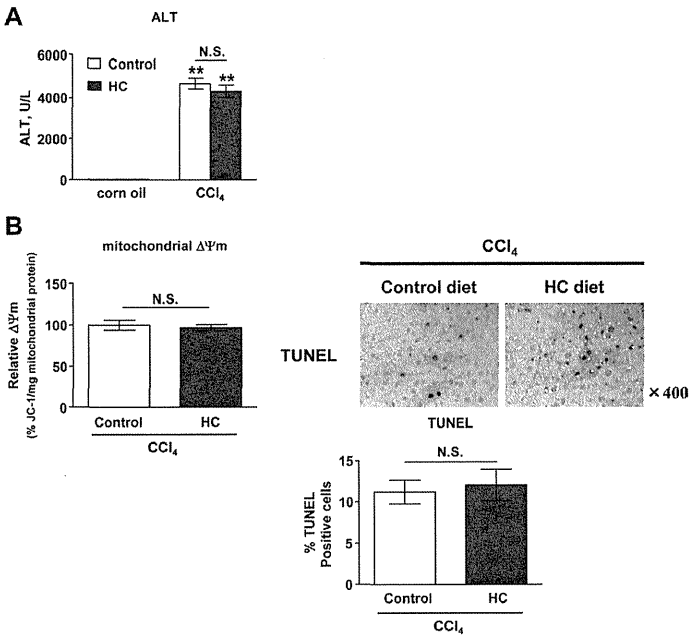

Supplementary Figure 2. Effects of the HC diet on acute liver injury induced by CCl_4 treatment. After being fed a control or an HC diet for 4 weeks, C57BL/6 mice were subjected to acute liver injury induced by a single injection of CCl_4 (N = 5/group). (*A*) Serum ALT activities (N = 5/group). (*B, left panels*) Electrochemical proton gradient of the inner mitochondrial membrane (N = 5/group). The calculated relative $\Delta\Psi$ was normalized to the values obtained in mice from the control diet–CCl_4 group. (*B, right panels*) The percentage of terminal deoxynucleotidyl transferase–mediated deoxyuridine nick-end labeling (TUNEL)-positive hepatocytes (N = 5/group) and the representative sections.

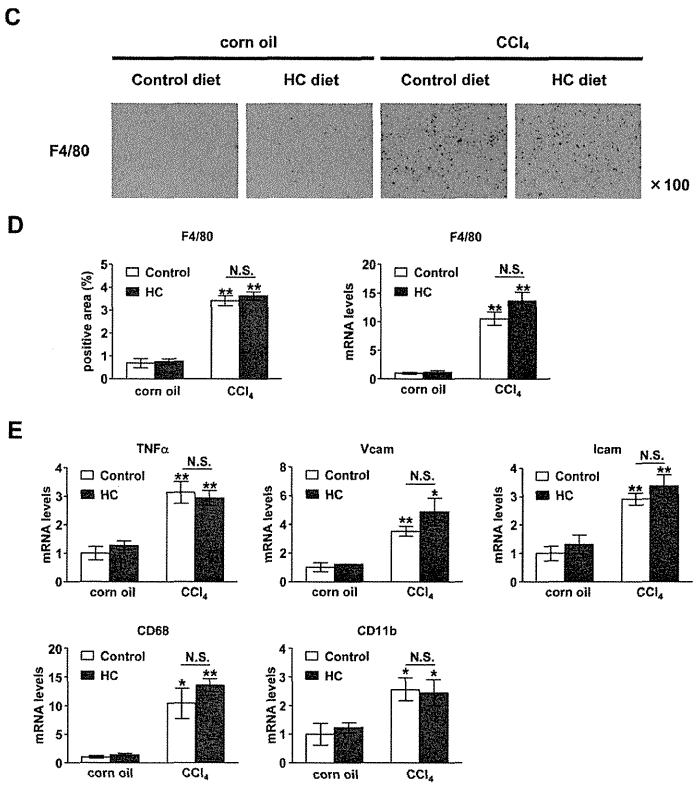

Supplementary Figure 2 (Cont'd.). (*C*) Immunohistochemical detection of F4/80-positive cells in livers. (*D*) Quantification of F4/80 by immunohistochemical staining and mRNA levels. (*E*) Hepatic expression of TNFα, vascular cell adhesion molecule-1 (VCAM-1), intercellular adhesion molecule-1 (ICAM-1), CD68, and CD11b mRNA (N = 5/group). $^{*}P < .05$ and $^{**}P < .01$ compared with control diet–corn oil group.

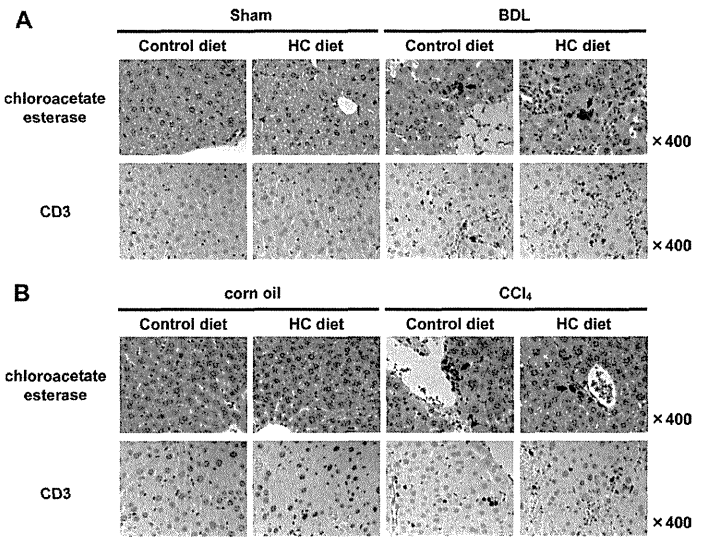

Supplementary Figure 3. Effects of the HC diet on the BDL- or CCl_4-mediated infiltration of T cells and neutrophils into the liver. After being fed a control or an HC diet for 4 weeks, C57BL/6 mice were subjected to (*A*) 3-week BDL or (*B*) CCl_4 treatment twice a week for 4 weeks to induce liver fibrosis (N = 5–7/group). (*Upper panels*) Staining by the naphtol AS-D chloroacetate esterase technique for detection of neutrophils and (*lower panels*) immunohistochemical staining for CD3 for detection of T cells.

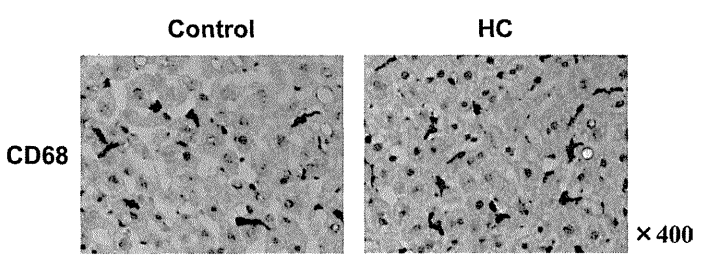

Supplementary Figure 4. HC diet did not induce the formation of hepatic macrophage foam cells. Immunohistochemical detection of CD68-positive cells in livers: mice fed a control diet (*left panel*) or an HC diet (*right panel*) for 8 weeks.

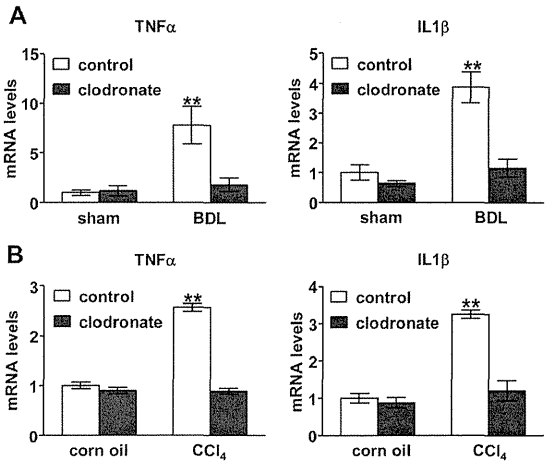

Supplementary Figure 5. Treatment with liposomal clodronate reversed BDL- and CCl_4-induced increase of TNFα and interleukin (IL)-1β mRNA expression in liver. WT C57BL/6 mice were injected with liposomal chlodronate (200 μL/mouse, intravenously) or vehicle. Thereafter, animals were subjected to (*A*) BDL or (*B*) CCl_4 intoxication to induce liver fibrosis. Hepatic expression of TNFα and IL-1β mRNA was shown. $^{**}P < .01$ compared with the (*A*) control diet–sham-operated group or the (*B*) control diet–corn oil group.

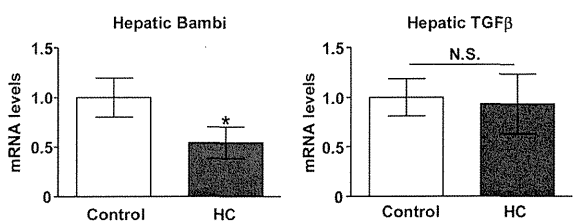

Supplementary Figure 6. Effects of the HC diet on hepatic expression of Bambi and TGFβ mRNA. Hepatic expression of Bambi and TGFβ mRNA (*N = 3/group*) after being fed a control or an HC diet for 4 weeks. $^{*}P < .05$ vs control diet group.

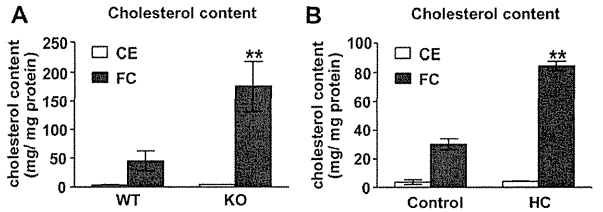

Supplementary Figure 7. Quantification of cellular FC and CE in late endosomes/lysosomes in HSCs. With late endosomes/lysosomes in WT HSCs, the mean (±SD) TC content was 48.46 ± 33.57 mg/mg cell protein. In late endosomes/lysosomes in NPC1 KO HSCs, the mean (±SD) TC content was increased significantly to 178.68 ± 81.39 mg/mg cell protein. Similarly, with late endosomes/lysosomes in HSCs from the control diet group, the mean (±SD) TC content was 33.82 ± 7.34 mg/mg cell protein. In late endosomes/lysosomes in HSCs from the HC diet group, the mean (±SD) TC content was increased significantly to 89.08 ± 6.57 mg/mg cell protein. (*A*) Quantification of FC and CE in late endosomes/lysosomes in HSCs from WT mice or NPC1-deficient mice. $^{**}P < .01$ vs WT mouse group. (*B*) The FC and CE levels in late endosomes/lysosomes in HSCs from control diet–fed mice or HC diet–fed mice. $^{**}P < .01$ vs control-diet group.

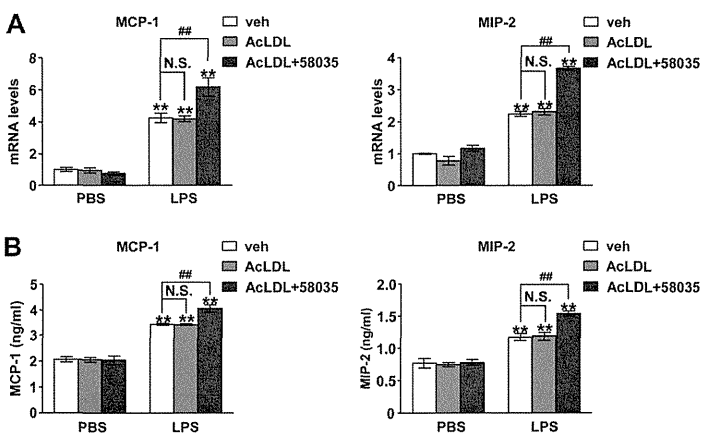

Supplementary Figure 8. FC, but not CE, promotes LPS-induced TLR4 signal transduction in HSCs. Paik et al[3] showed that LPS acts directly through TLR4 and then activates nuclear factor-κB to induce the production of inflammatory cytokines, including interleukin (IL)-8 and monocyte chemoattractant protein-1 (MCP-1), in human activated HSCs. Seki et al[4] also showed a strong up-regulation of MCP-1 and macrophage inflammatory protein-2 (MIP-2: mouse homologue of human IL-8) mRNA in mouse HSCs after LPS stimulation. Based on these reports, we evaluated the LPS responsiveness of HSCs loaded with FC using 2 highly quantitative methods: real-time polymerase chain reaction (PCR) and enzyme-linked immunosorbent assay (ELISA) of TLR4-induced inflammatory cytokines such as MCP-1 and MIP-2. (*A*) Expression of MCP-1 and MIP-2 mRNA in primary HSC cultures. HSCs were incubated with vehicle, AcLDL (50 μg/mL), or AcLDL plus compound 58035 (10 μg/mL) for 16 hours, and then treated with LPS (100 ng/mL) or not for 6 hours (N = 5–7/group). (*B*) Secreted MCP-1 and MIP-2 were quantified by ELISA. HSCs were incubated with vehicle, AcLDL, or AcLDL plus compound 58035 for 16 hours, and then treated with LPS or not for 24 hours (N = 5/group). $^{**}P < .01$ vs the *corresponding culture without LPS treatment in each group.* $^{\#\#}P < .01$ *vs the LPS-treated control culture.*

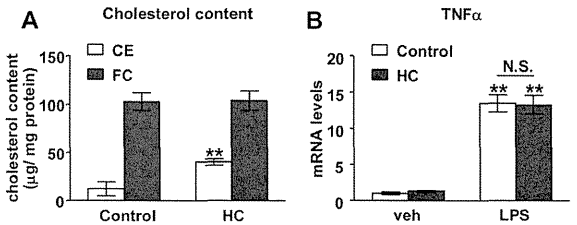

Supplementary Figure 9. Effects of the HC diet on cholesterol contents in Kupffer cells. We determined the level of cholesterol inside Kupffer cells. With Kupffer cells from the control diet group, the mean (±SD) TC content was 115.03 ± 22.61 μg/mg cell protein. In Kupffer cells from the HC diet group, the mean (±SD) TC content was increased significantly to 144.11 ± 38.83 μg/mg cell protein. (*A*) Quantification of cellular FC and CE in Kupffer cells from control diet–fed or HC diet–fed mice. Cholesterol concentrations were expressed as micrograms per milligrams of cellular proteins (N = 4/group). $^{**}P < .01$ vs the control diet group. (*B*) Expression of TNFα mRNA in primary Kupffer cell cultures (N = 5/group). Kupffer cells isolated from control diet–fed or HC diet–fed mice were treated with LPS (100 ng/mL) for 6 hours. $^{**}P < .01$ vs the control diet–control culture.

Supplementary Table 1. Effects of the HC Diet on Body Weight, Liver Weight, and Serum Lipid Levels

	Sham				BDL			
	Control diet		HC diet		Control diet		HC diet	
	Mean	SEM	Mean	SEM	Mean	SEM	Mean	SEM
Body weight, g	28.2	0.3	27.2	0.6	27.5	2.3	21.8	0.3
Liver weight, g	1.4	0.1	1.2	0.1	1.7	0.2	2.1	0.2
Serum TG level, mg/dL	130.2	4.5	125.4	6.9	72.1	8.6	75.5	15.6
Serum TC level, mg/dL	103.2	9.8	135.0[a]	3.0	150.7	22.6	407.0[b]	17.7
Serum glucose level, mg/dL	116.6	5.4	120.8	17.6	85.3	26.7	103.0	23.0
	Corn oil				CCl_4			
Body weight, g	23.8	0.5	24.3	0.9	23.2	0.2	24.3	0.6
Liver weight, g	1.1	0.0	1.2	0.1	1.1	0.1	1.2	0.0
Serum TG level, mg/dL	229.4	19.6	173.8	20.6	170.8	16.9	193.5	12.0
Serum TC level, mg/dL	120.0	4.5	138.5[c]	9.0	118.0	4.1	143.8[d]	8.2
Serum glucose level, mg/dL	102.2	9.3	88.3	5.9	86.3	6.9	103.5	12.1

SEM, standard error of the mean.
[a] $P < .05$ vs the control diet-sham-operated group.
[b] $P < .01$ vs the control diet-BDL-operated group.
[c] $P < .05$ vs the control diet-corn oil group.
[d] $P < .05$ vs the control diet-CCl_4 group.

RESEARCH PAPER
Oncolmmunology 1:5, 581–592; August 2012; © 2012 Landes Bioscience

Cross-priming for antitumor CTL induced by soluble Ag + polyI:C depends on the TICAM-1 pathway in mouse CD11c$^+$/CD8α$^+$ dendritic cells

Masahiro Azuma, Takashi Ebihara,[†] Hiroyuki Oshiumi, Misako Matsumoto and Tsukasa Seya*

Department of Microbiology and Immunology; Hokkaido University Graduate School of Medicine; Sapporo, Japan

[†]Current affiliation: Howard Hughes Medical Institute; Washington University School of Medicine; St. Louis, MO USA

Keywords: cross-presentation, dendritic cell, TLR3, TICAM-1 (TRIF), tumoricidal CTL

Abbreviations: APC, antigen-presenting cells; CTL, cytotoxic T lymphocytes; DAMP, damage-associated molecular pattern; DC, dendritic cells; IFN, interferon; IPS-1, IFNβ promoter stimulator-1; MDA5, melanoma differentiation associated gene 5; Mf, macrophages; NK, natural killer; OVA, ovalbumin; PAMP, pathogen-associated molecular pattern; PRR, pattern-recognition receptors; PV, poliovirus; RIG-I, retinoic acid inducible gene-1; SL8, an OVA tetramer; TICAM-1, Toll-IL-1 receptor homology domain-containing molecule-1; TLR, Toll-like receptor; WT, wild-type

PolyI:C is a nucleotide pattern molecule that induces cross-presentation of foreign Ag in myeloid dendritic cells (DC) and MHC Class I-dependent proliferation of cytotoxic T lymphocytes (CTL). DC (BM or spleen CD8α$^+$) have sensors for dsRNA including polyI:C to signal facilitating cross-presentation. Endosomal TLR3 and cytoplasmic RIG-I/MDA5 are reportedly responsible for polyI:C sensing and presumed to deliver signal for cross-presentation via TICAM-1 (TRIF) and IPS-1 (MAVS, Cardif, VISA) adaptors, respectively. In fact, when tumor-associated Ag (TAA) was simultaneously taken up with polyI:C in DC, the DC cross-primed CTL specific to the TAA in a syngenic mouse model. Here we tested which of the TICAM-1 or IPS-1 pathway participate in cross-presentation of tumor-associated soluble Ag and retardation of tumor growth in the setting with a syngeneic tumor implant system, EG7/C57BL6, and exogenously challenged soluble Ag (EG7 lysate) and polyI:C. When EG7 lysate and polyI:C were subcutaneously injected in tumor-bearing mice, EG7 tumor growth retardation was observed in wild-type and to a lesser extent IPS-1$^{-/-}$ mice, but not TICAM-1$^{-/-}$ mice. IRF-3/7 were essential but IPS-1 and type I IFN were minimally involved in the polyI:C-mediated CTL proliferation. Although both TICAM-1 and IPS-1 contributed to CD86/CD40 upregulation in CD8α$^+$ DC, H2K^b-SL8 tetramer and OT-1 proliferation assays indicated that OVA-recognizing CD8 T cells predominantly proliferated in vivo through TICAM-1 and CD8α$^+$ DC is crucial in ex vivo analysis. Ultimately, tumor regresses > 8 d post polyI:C administration. The results infer that soluble tumor Ag induces tumor growth retardation, i.e., therapeutic potential, if the TICAM-1 signal coincidentally occurs in CD8α$^+$ DC around the tumor.

Introduction

Cytotoxic T lymphocytes (CTL) and natural killer (NK) cells are two major effectors for antitumor cellular immunity. These effectors are driven through activation of dendritic cells (DC) and/or macrophages (Mf), which is mediated by pattern-recognition receptors (PRRs) for the recognition of microbial patterns.[1,2] Antigen (Ag) presentation and upregulation of NK cell-activating ligands are major events induced in DC/Mf in response to PRRs, which link to evoking CTL- and NK-antitumor immunity, respectively. The immune-potentiating function of specific components of the classical adjuvants are largely attributable to the ligand activity of PRRs (CpG DNA/TLR9, polyI:C/TLR3, monophosphoryl lipid (MPL) A/TLR4, Pam2/TLR2, etc.).[3] That is, the DC/Mf competent to drive effectors are generated through PRR signal in inflammatory nest where affected cells and recruited immune cells encounter exogenous or endogenous PRR ligands. Since studying the functional properties of PRRs in tumor immunity is on the way using a variety of possible ligands and cell biological analyses, immune responses reflecting the total adjuvant potential around Ag-presenting cells (APC) in local inflammatory nests are not always elucidated even in mice.

RNA-sensing PRR pathways, including TLR3-TICAM-1, TLR7-MyD88 and RIG-I/MDA5-IPS-1 participate in driving Type I IFN induction and cellular immunity in DC subsets.[1,4,5] Type I IFN and the IFNAR pathway in DC and other cells reportedly evoke and amplify T cell immunity.[5,6] TLR7 resides exclusively in plasmacytoid DC[7] whereas TLR3 mainly exists in

*Correspondence to: Tsukasa Seya; Email: seya-tu@pop.med.hokudai.ac.jp
Submitted: 02/04/12; Revised: 03/02/12; Accepted: 03/02/12
http://dx.doi.org/10.4161/onci.19893

©2012 Landes Bioscience. Do not distribute.

myeloid DC/Mf and epithelial cells.[8] They are localized on the membrane of the endosome and deliver the signal via their adaptors, MyD88 and TICAM-1.[7,8] RIG-I and MDA5 are ubiquitously distributed to a variety of mouse cells and signal the presence of cytoplasmic viral products through IPS-1.[9] Thus, TLR3 and RIG-I/MDA5 are candidates associated with DC maturation to drive effector cells.[10] Indeed, viral dsRNA analog, polyI:C, is a representative ligand for TLR3 and MDA5 and induces polyI:C-mediated DC-NK reciprocal activation.[11,12] These are also true in human DC.[13]

The point of this study is by which pathway antitumor CTL are induced for tumor regression in a mouse tumor-implant model. It has been postulated that DC present exogenous tumor Ag to the MHC Class I-restricted Ag-presentation pathway and proliferate CD8 T cells specific to the extrinsic Ag. When tumor cells provide soluble and insoluble exogenous Ag, this Class I Ag presentation occurs mostly TAP/proteasome-dependent, suggesting the pathway partly sharing with that for endogenous Ag presentation. This DC's ability to deliver exogenous Ag to the pathway for MHC Class I-restricted Ag presentation has been described as cross-presentation.[14] DC cross-presentation leads to the cross-priming and proliferation of Ag-specific CD8 T cells in vivo and in vitro.[14-18] A variety of PAMP[15,16] and intrinsic DAMP[17] as well as other factors including Type I IFN,[5,18] CD4$^+$ T cells[19] and NKT cells[20] augment cross-priming in tumor-bearing mice. However, by what molecular mechanism polyI:C enhances CTL induction in tumor-bearing mice remains largely unsettled.

Here, we made an EG7 tumor-implant mouse system and treated the mice with s.c.-injected ovalbumin (OVA)-containing cell lysates (Ag) and polyI:C. Spleen CD8α$^+$ DC turn CTL-inducible when stimulated with Ag and polyI:C. In either case of s.c., i.p., or i.v. injection of polyI:C, the TLR3/TICAM-1 pathway predominantly participates in CD8α$^+$ DC cross-priming and antitumor CTL induction. Earlier studies using non-tumor models, suggested that both TLR3 and MDA5 appeared to participate in polyI:C-dependent CTL induction.[21] TLR3 is predominantly involved in primary Ag response and Th1 skewing,[22] while MDA5 participates in secondary Ag response.[23] Importance of TLR3 in induction of cross-priming was first suggested by Schulz et al., who used OVA/polyI:C-loaded or virus-infected xenogenic (Vero) cells and mouse DC.[16] Here we demonstrate that the antitumor polyI:C activity is sustained by the TICAM-1 pathway in any route of injection in tumor-implant mice: antitumor CTL responses are mostly abrogated in TICAM-1$^{-/-}$ but not IPS-1$^{-/-}$ mice.

Results

Properties of EG7 tumor with high MHC in tumor-loading mice. The properties of the EG7 line we used are consistent with those reported previously.[24,25] It expressed high MHC Class I (H2-Kb) and no Qa-1b or Rae-1 (**Fig. S1**). The expression levels of these proteins were barely changed before and after implantation of EG7 cells into mice. Cell viability was not affected by in vitro stimulation with polyI:C only (**Fig. S1B**). However, a batch-to-batch difference of cell viability may have affected the rate of tumor growth in each mouse tumor-implant experiment.

CD8$^+$ T cells are responsible for tumor retardation by polyI:C. EG7 cells (2×10^6) were inoculated into the back of C57BL/6 (WT), and the indicated reagents were subcutaneously (s.c.) injected around the EG7 tumor (**Fig. 1A**). Growth retardation of tumor was observed by treatment with polyI:C or polyI:C plus EG7 lysate (**Fig. 1A**). EG7 lysate only had no effect on tumor regression. When CD8β$^+$ T cells were depleted before EG7 lysate/polyI:C treatment, polyI:C-mediated tumor growth suppression was cancelled (**Fig. 1A**), suggesting the participation of CD8 T cells in tumor growth suppression. The therapeutic potential of polyI:C appeared to be more reproducible in the presence of EG7 lysate than in the absence, judged from the increases of activated CD8$^+$ T cells (**Fig. 1B**) and cytotoxic activity (**Fig. 1C**) of LN T cells isolated from the mice sacrificed after the last therapy. Yet, the EG7 Ag could be more or less supplied from the implant tumor. NK1.1$^+$ cells did not participate in this EG7 tumor regression in this setting (data not shown).

Since EG7 lysate contains OVA, OVA-specific T cells in draining LN and spleen of the WT mice were counted by tetramer assay after the last therapy (**Fig. S2A and B**). The numbers of tetramer-positive cells were prominently increased in LN and spleen in mice with EG7 lysate and polyI:C. We confirmed the importance of simultaneous administration of Ag plus polyI:C for OVA-specific CTL induction as in **Figure S2C**, where pure Ag (OVA) was used instead of EG7 lysate for immunotherapy. The polyI:C adjuvant function appeared to be more efficient in the mixture of pure Ag than in polyI:C alone. Tumor regression (**Fig. S2C**) and OVA-specific CTL induction (**Fig. S2D**) were clearly observed in this additional experiment. To obtain reproducible data, we employed the EG7 lysate/polyI:C combination therapy as follows.

IFN-inducing pathways are involved in PolyI:C-derived EG7 growth retardation. We next inoculated EG7 cells (2×10^6) into the back of C57BL/6 (WT), TICAM-1$^{-/-}$, IPS-1$^{-/-}$, or TICAM-1/IPS-1 double-deficient (DKO) mice (**Fig. 2**). We s.c. administered EG7 lysate with or without polyI:C around the tumor. The EG7 lysate was the soluble fraction of EG7 which removed insoluble debris by centrifugation. The EG7 lysate contained unprecipitated micro-debris and soluble Ag. No other emulsified reagent was added for immunization. Thus, the adjuvant function of polyI:C per se is reflected in the tumor growth, although polyI:C had to be injected into mice twice a week. Retardation of tumor growth was observed > 8 d after immunization with EG7 lysate + polyI:C in WT mice, though no growth retardation without polyI:C (**Fig. 2A**). The polyI:C-mediated tumor growth suppression was largely abrogated in TICAM-1$^{-/-}$ (**Fig. 2B**) and to a lesser extent in IPS-1$^{-/-}$ mice (**Fig. 2C**), and completely in TICAM-1/IPS-1 DKO mice (**Fig. 2D**). Hence, TICAM-1 plays an important role in inducing polyI:C-mediated tumor growth retardation in the s.c. setting we employed.

CD8 T cell activation induced by the TICAM-1 pathway. CD8 T cell activation in the inguinal LN was tested with polyI:C + EG7 lysate in EG7 tumor-bearing mice using CD69 as an activating marker. Twenty-four hours after the last polyI:C + EG7 sec.c. treatment, cells were harvested from the LN excised (**Fig. 3A**). FACS profiles of total cells from each mouse group are shown in **Fig. S3**. By combination therapy with EG7 lysate and polyI:C, T cells were activated in WT and IPS-1$^{-/-}$ mice, but the proportion of CD8 T cells was not affected by the therapy (**Fig. S4A**). Under the same conditions, T cells were barely activated in TICAM-1$^{-/-}$ mice in response to polyI:C (**Fig. 3A**). The proportion of CD69$^+$ cells are indicated in **Figure 3B**. IL-2 (**Fig. 3C**) and IFNγ (**Fig. S4B**) were highly induced in the WT and IPS-1$^{-/-}$ LN cells, while they were not induced in TICAM-1$^{-/-}$ or DKO cells. IFNγ levels were upregulated only in polyI:C-treated tumor-bearing mice, although the WT > IPS-1$^{-/-}$ profile for IFNγ production was reproducibly observed (**Fig. S4B**).

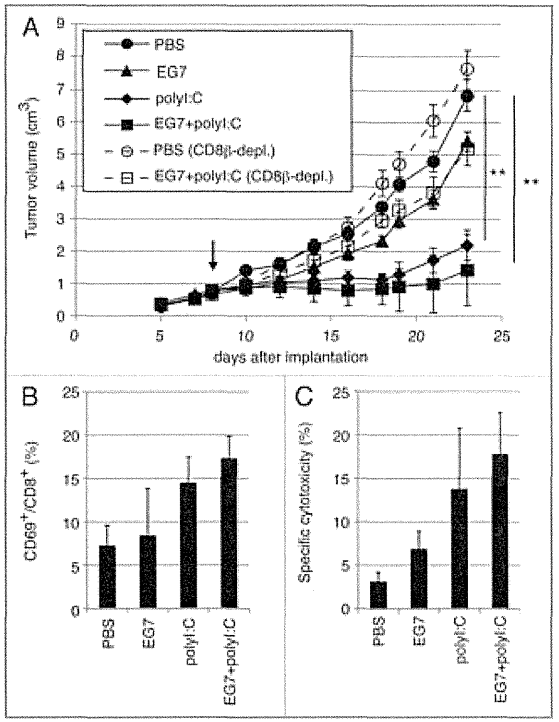

Figure 1. PolyI:C induces CTL-mediated tumor regression. (A) WT mice were challenged with EG7 cells and were treated with PBS (●), EG7 lysates (▲), polyI:C (◆) and EG7 lysates + polyI:C (■). The adjuvant therapy was started at the time indicated by the arrow and the indicated reagents injected twice per week. One of the two PBS groups (○) and one of the two EG7 lysates + polyI:C groups (□) were treated with anti-CD8β ascites in order to deplete CD8$^+$ T cells once a week. Each group had 3–5 mice. (B) Draining inguinal LNs were harvested 24 h after the last treatment and the proportion of CD69-expressing CD8$^+$ cells were counted. (C) LN cells were co-cultured with MMC-treated EG7 cells for 3 d and subjected to ^{51}Cr release assay to evaluate CTL activity. E/T = 50. All error bars used in this figure show ± SEM. Data are representative of two independent experiments. One-way analysis of variance (ANOVA) with Bonferroni's test was performed to analyze statistical significance. **, $p < 0.01$.

In vivo proliferation of CD8 T cells judged by tetramer assay and IFNγ induction. We next tested whether i.p. injection of polyI:C plus OVA induces CTL proliferation. PolyI:C and OVA were i.p. injected into mice and the polyI:C-dependent cross-priming of CD8 T cells were examined using the OVA tetramer assay. OVA-specific CD8 T cells were clonally proliferated in WT and IPS-1$^{-/-}$ mice, but not in TICAM-1/IPS-1 DKO and IRF-3/7$^{-/-}$ mice (**Fig. 4A**). Proliferation of OVA-specific CD8 T cells were severely suppressed in TICAM-1$^{-/-}$ mice (**Fig. 4A**), suggesting that polyI:C-mediated cross-priming of CD8 T cells largely depends on the TICAM-1 pathway followed by IRF-3/7 activation in the i.p. route. The results were reproduced in additional experiments using more mice (**Fig. 4B**) and TLR3$^{-/-}$ mice (**Fig. S5A and B**). The polyI:C cytokine response, where IFNα is IPS-1-dependent while IL-12p40 is TICAM-1-dependent, was also confirmed in serum level by polyI:C i.p. injection (**Fig. S5E**). Specific induction of IFNγ (**Fig. 4C**) was also observed in parallel with the results of **Figure 4A**.

Whether or not i.v. injection of polyI:C plus OVA induces Ag-specific CTL and cytotoxicity was next checked. OVA-specific OT-1 proliferation and cytotoxicity (**Fig. 4D and E**) were observed in in vivo analyses of WT and IPS-1$^{-/-}$ CD8 T cells but not of TICAM-1$^{-/-}$, TICAM-1/IPS-1 DKO, and IRF-3/7$^{-/-}$ mice in the i.v. setting.

Since TICAM-1 is the adaptor for TLR3 as well as cytoplasmic helicases,[24] we confirmed the level of cross-priming being decreased in TLR3$^{-/-}$ mice and an expected result was obtained (**Fig. S5A and B**). Furthermore, in IFNAR$^{-/-}$ mice, OVA-specific CTL induction was slightly reduced compared with that in WT mice, but higher than in TICAM-1$^{-/-}$ mice (**Fig. S5C and D**). Hence, in vivo cross-presentation induced by polyI:C mostly depends on the TLR3-TICAM-1 pathway followed by transcriptional regulation by IRF-3/7 in any administration route, and is further promoted by Type I IFN presumably produced by the stromal cells through the IPS-1 pathway.[26]

IPS-1 induces DC maturation but not cross-priming in vivo. Spleen DC maturation by i.v.-injected polyI:C was tested ex vivo using CD8α$^+$ DC and CD8α$^-$ DC isolated from WT or KO mice with no tumor as indicated in **Figure 5A**. The maturation markers CD86 and CD40 were upregulated on both CD8α$^+$ and CD8α$^-$

©2012 Landes Bioscience. Do not distribute.

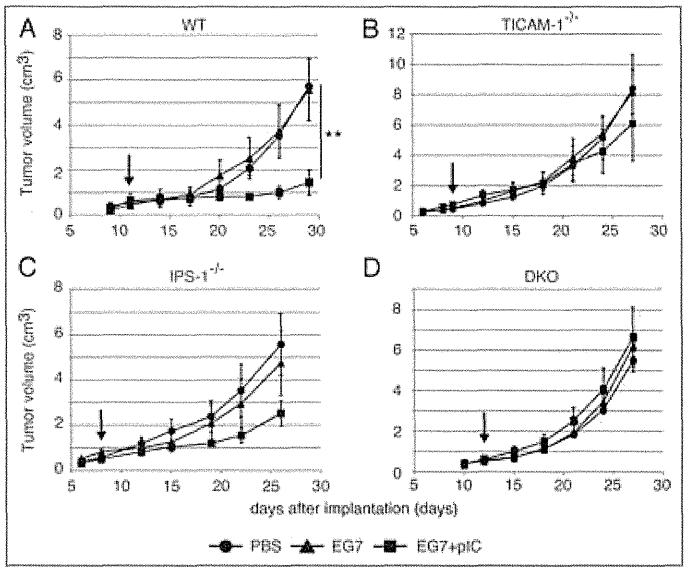

Figure 2. PolyI:C-induced tumor retardation is dependent on the TICAM-1 pathway. Antitumor effect of polyI:C on various KO mice were evaluated by using in vivo mouse tumor implant model. EG7 cells were inoculated to WT (A), TICAM-1$^{-/-}$ (B), IPS-1$^{-/-}$ (C) and DKO mice (D) on day 0. PBS (●), EG7 lysates (▲) or EG7 lysates + polyI:C (■) were s.c. administered around the tumor. The adjuvant therapies were started at the time indicated by the arrows and injected twice per week. Each group have 3–4 mice and error bar shows ± SEM. Data are representative of two independent experiments. **, $p < 0.01$

DC from WT mice when they were stimulated with OVA and polyI:C. Treatment of DC with OVA only did not induce upregulation of CD86 and CD40. Although the expression levels of CD86 and CD40 were a little less in CD8α$^+$ and CD8α$^-$ DC from TICAM-1$^{-/-}$ or IPS-1$^{-/-}$ mice than those from WT mice, both CD86 and CD40 were sufficiently upregulated even in the abrogation of either one pathway in polyI:C-injected mice. The CD86 and CD40 shifts were completely abolished in DKO mice (**Fig. 5A**). Thus, the TICAM-1 pathway participates in both potent co-stimulation and cross-priming, while the IPS-1 pathway mainly participates only in integral co-stimulation in myeloid DC.

We next assessed in vitro proliferation of OT-1 cells. CD8α$^+$ and CD8α$^-$ DC were prepared from PBS, polyI:C, OVA and OVA/polyI:C-treated mice, and mixed in vitro with CFSE-labeled OT-1 cells. WT, TICAM-1$^{-/-}$ and IPS-1$^{-/-}$ mice were used for this study. OT-1 proliferation was observed with CD8α$^+$ DC but not CD8α$^-$ DC when OVA + polyI:C was injected (**Fig. 5B**). Furthermore, the OT-1 proliferation barely occurred in the mixture containing TICAM-1$^{-/-}$ CD8α$^+$ DC. Thus, OT-1 proliferation is triggered by the TICAM-1 pathway in CD8α$^+$ DC. Again, IPS-1 had almost no effect on OT-1 proliferation with CD8α$^+$ DC in this setting. In the mixture, IFNγ was produced in the supernatants of WT and IPS-1$^{-/-}$ CD8α$^+$ DC but not TICAM-1$^{-/-}$ DC by stimulation with OVA + polyI:C (**Fig. 5C**). No IFNγ was produced in the supernatants of CD8α$^-$ DC even from WT mice, which results are in parallel with those of OT-1 proliferation. In any case irrespective of tumor-bearing or not, Ag, polyI:C and the TICAM-1 pathway are mandatory for CD8α$^+$ DC to cross-prime and proliferate OVA-specific CD8 T cells.

We checked the TICAM-1- or IPS-1-specific gene expressions related to Type I IFN and MHC Class I presentation using genechip and qPCR (**Fig. S6**). PolyI:C-mediated upregulation of *Tap1*, *Tap2* and *Tapbp* messages diminished in TICAM-1$^{-/-}$ BMDC (**Fig. S6A**). The levels of these genes were hardly affected in IPS-1$^{-/-}$ BMDC (data not shown). PolyI:C-mediated upregulation was observed with MDA5 (*Ifih1*) in CD8α$^-$ and CD8α$^+$ DCs (**Fig. S6B**). Surprisingly, other factors including TLR3, TICAM-1 and MAVS messages were all downregulated in response to polyI:C in CD8α$^+$ DC (**Fig. S6B**), for the reason as yet unknown.

Effect of TLR3-mediated IFN-inducing pathway on anti-tumor CTL induction. PolyI:C is a dsRNA analog capable of incorporating into the endosome and cytoplasm by exogenous administration in vitro.[27,28] However, no evidence has been proposed that polyI:C is internalized into the endosome of

©2012 Landes Bioscience. Do not distribute.

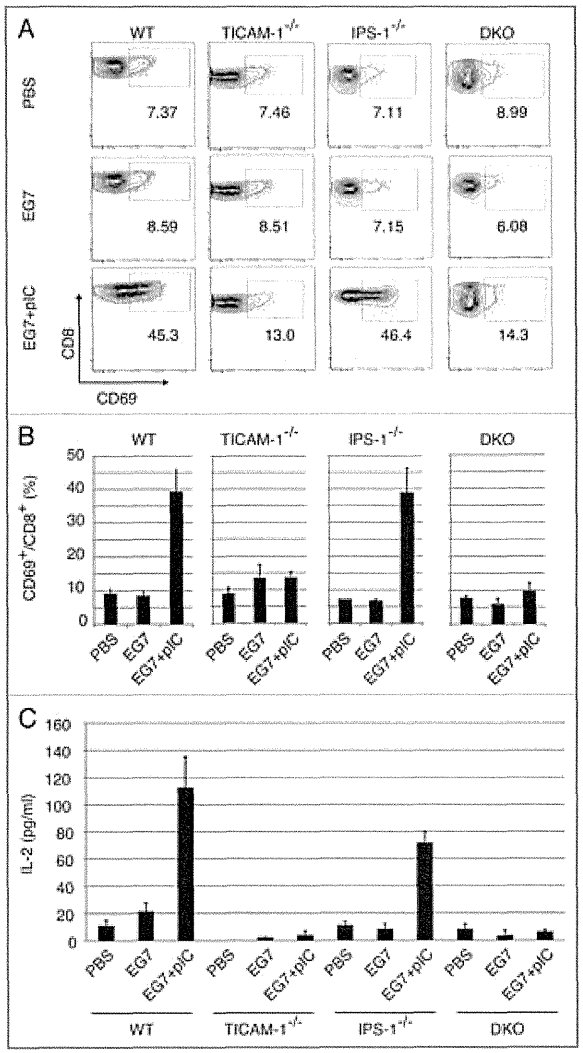

Figure 3. CD8 T cells in the draining LNs are activated through the TICAM-1 pathway by polyI:C. Draining inguinal LNs were harvested from tumor-bearing mice 24 h after the last treatment. LN cells were stained with CD3ε, CD8α and CD69, and the cells gated on CD3ε$^+$CD8α$^+$ are shown (A). Spleen cells in each group of mice were stained separately, the CD8 levels in gated cells being variably distributed in FACS analyses. The average frequency of activated CD8 T cells defined by CD69 expression is shown (B). Alternatively, LN cells from the indicated mice were cultured for further 3 d in vitro and IL-2 production was measured by CBA assay (C).

©2012 Landes Bioscience. Do not distribute.

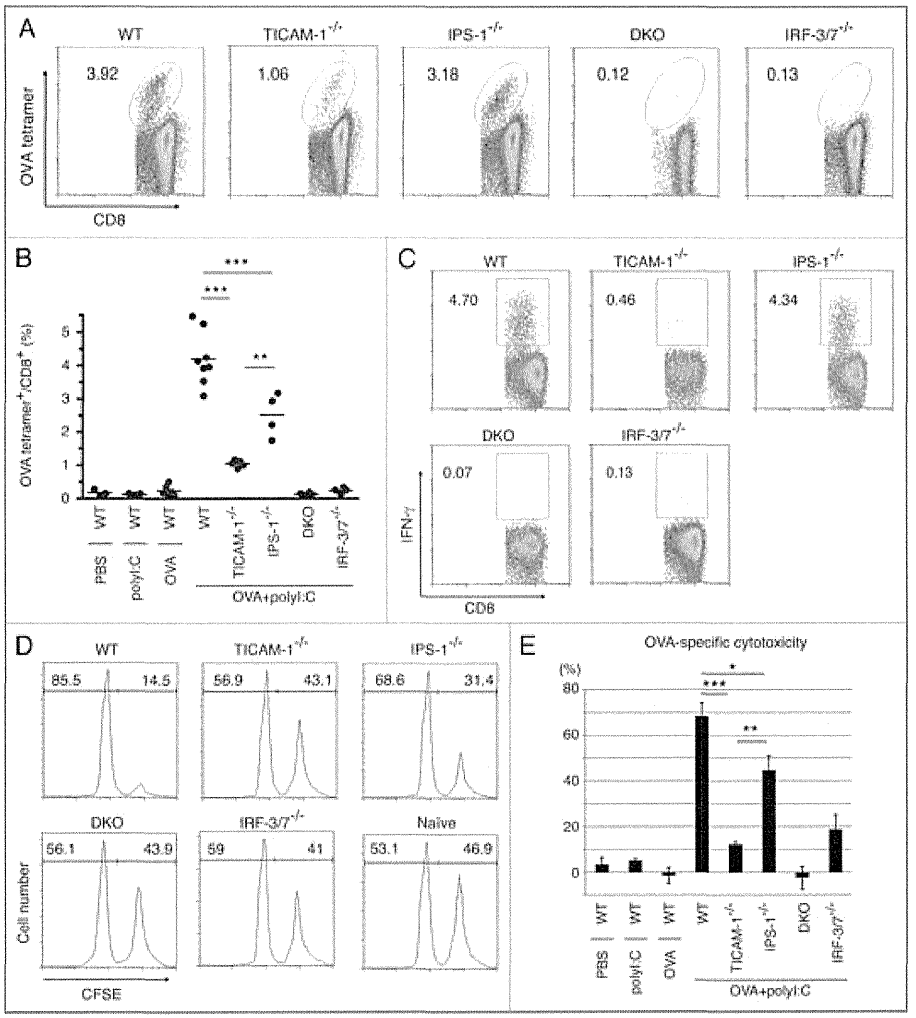

Figure 4. TICAM-1 and IRF-3/7 are essential for polyI:C-induced antigen-specific CTL expansion. WT, TICAM-1$^{-/-}$, IPS-1$^{-/-}$, TICAM-1/IPS-1 DKO and IRF-3/7$^{-/-}$ mice were i.p. administered with the combination of OVA and polyI:C. After 7days, splenocytes were harvested and stained with CD8α and OVA tetramer (A). The average percentages of OVA-specific CTL are shown (B). Alternatively, splenocytes were cultured in vitro in the presence of SL8 for 8 h and IFNγ production was measured by intracellular cytokine staining (C). To assess the killing activity, in vivo CTL assay was performed. The combinations of OVA and polyI:C were administered i.v. to each group of mice and 5 d later, cytotoxicity was measured (D). The data shown are collaborate or representative of at least three independent experiments. One-way analysis of variance (ANOVA) with Bonferroni's test was performed to analyze statistical significance. *, $p < 0.05$; **, $p < 0.01$; ***, $p < 0.001$.

©2012 Landes Bioscience. Do not distribute.

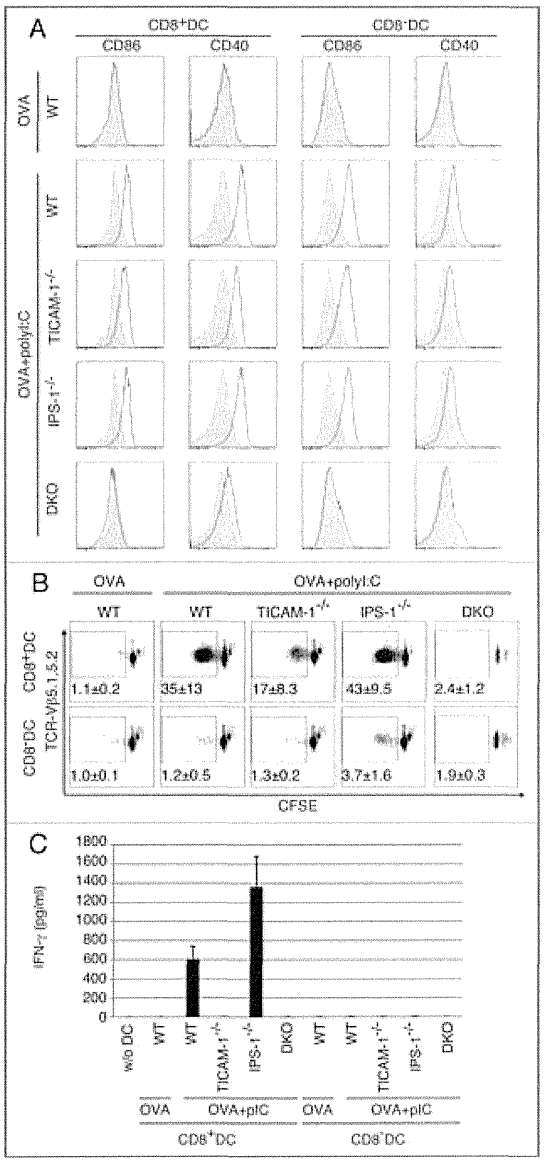

Figure 5. TICAM-1 in CD8α$^+$ DC is more important than IPS-1 in polyI:C-induced cross-priming. OVA and polyI:C were administered i.v. and 4 h later, CD8α$^+$ and CD8α$^-$ DC were isolated from the spleen. CD86 and CD40 expressions were determined by FACS (A). Filled gray and black line show isotype control and target expression, respectively. Alternatively, CD8α$^+$ and CD8α$^-$ DC were co-cultured with CFSE-labeled RAG2$^{-/-}$/OT-1 T cells for 3 d. The cross-priming activity of each DC subset was determined with sequential dilution of CFSE (B) and IFNγ production (C). IFNγ was measured by CBA assay. The data shown are representative of two independent experiments. Err bar shows SD.

CD8α$^+$ DC where TLR3 is expressed in vivo. Peritoneal (PEC) Mf and bone marrow-derived DC[22] usually phagocytoze polyI:C and deliver them into the endosome. In mouse CD8α$^+$ DC direct internalization of polyI:C has remain unproven. Using labeled polyI:C and anti-mouse TLR3 mAb, 11F8,[22] we checked whether the exogenously-added polyI:C encountered with TLR3 in CD8α$^+$ DC in vitro. TLR3 (green) was merged with TexasRed-polyI:C 30–120 min after polyI:C stimulation in the culture (**Fig. 6A**). The quantities of CD8α$^+$ and CD8α$^-$ DC where FITC-polyI:C was incorporated were determined by FACS analysis (**Fig. 6B**). Thus, the process by which polyI:C injected reaches the endosomal TLR3 is delineated in the CD8α$^+$ DC.

Discussion

PolyI:C is an analog of virus dsRNA, and acts as a ligand for TLR3 and RIG-I/MDA5. PolyI:C has been utilized as an adjuvant for enhancement of antitumor immunity for a long time.[29] However, the mechanistic background of the therapeutic potentials of polyI:C against cancer has been poorly illustrated. It induces antitumor NK activation through DC-NK cell-to-cell interaction when CD8α$^+$ DC TLR3 is stimulated in the spleen.[11] Besides myeloid cells, however, some tumor cell lines express TLR3 and dsRNA targeting tumor cells may affect the growth rate of tumors,[30] where the receptor-interacting protein (RIP) pathway is involved downstream of TICAM-1.[31] Here we showed evidence that polyI:C injection facilitates maturation of TLR3-positive CD8α$^+$ DC (i.e., APC) to trigger CTL induction against exogenous soluble Ags including EG7 lysate or OVA. The TICAM-1 adaptor for TLR3 and IRF-3/7 are involved in the cross-presentation signal in CD8α$^+$ DC, but the molecule/mechanism downstream of TICAM-1 that governs cross-presentation remains elusive. Since most of the tumor-associated Ags (TAA) are predicted to be liberated from tumor cells

©2012 Landes Bioscience. Do not distribute.

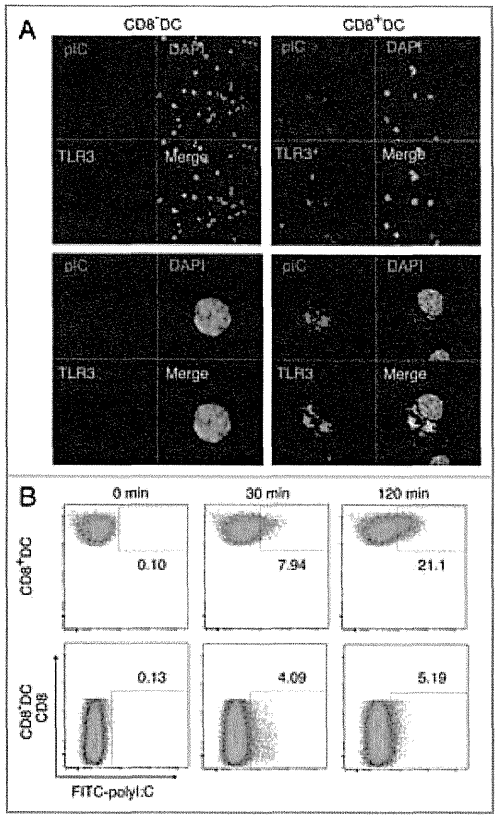

Figure 6. PolyI:C encounters TLR3 in CD8α⁺ DC. CD8α⁺ and CD8α⁻ DC were isolated by FACSAriall and stimulated with 20 μg/ml TexasRed-polyI:C for 2 h. Then cells were stained with Alexa647-antiTLR3 and subjected to confocal microscopic analysis (A). Alternatively, splenic DC isolated by MACS were incubated with FITC-polyI:C for the time shown in figure and analyzed the degrees of polyI:C uptake by FACS (B). Data shown are the representative of three independent experiments.

as soluble Ags, the TICAM-1 pathway in CD8α⁺ DC would be crucial for driving of tumor-specific CTL around the tumor microenvironment. In any route of polyI:C injection, this is true as shown first in this study. Although TICAM-1 is an adaptor of other cytoplasmic sensors, DDX1, DDX21 and DHX36,[32] the antitumor CTL responses are merely relied on TLR3 of CD8α⁺DC in this system. Taken together with previous reports,[11,12] TICAM-1 signaling triggers not only NK activation but also CTL induction.

TLR3 and MDA5 are main sensors for dsRNA and differentially distributed in myeloid cells.[33,34] TLR3 is limitedly expressed in myeloid, epithelial and neuronal cells,[33] whereas MDA5 is ubiquitously expressed including non-myeloid stromal cells.[33] Several reports suggested that i.v. injection of polyI:C predominantly stimulate the stromal cells which express IFNAR,[26] thereby robust type I IFN are liberated from these cells to be a systemic response including cytokinemia and endotoxin-like shock.[35,36] Both TLR3 and MDA5 link to the IRF-3/7-activating kinases leading to the production of IFNα/β.[37,38] Once IFNα/β are released, IFNAR senses it to amplify the Type I IFN production,[39] and reportedly this amplification pathway involves cross-priming of CD8 T cells in viral infection.[18] Tumor progression or metastasis can be suppressed through the IFNAR pathway.[40] These scenarios may be right depending on the conditions employed. Our message is related to what signal pathway is fundamentally required for induction of antitumor CTL in DC. The CTL response is almost completely abrogated in TICAM-1$^{-/-}$ and IRF-3/7$^{-/-}$ mice, but largely remains in IPS-1$^{-/-}$ and IFNAR$^{-/-}$ mice when Ag and polyI:C are extrinsically administered. The results are reproducible in some other tumor-implant models (data not shown), and even in IFNAR$^{-/-}$ mice, TICAM-1-specific genes are upregulated to confer tumor cytotoxicity (**Fig. S6**, Azuma et al., unpublished data). In addition, the upregulation of these genes is independent of IPS-1 knockout in DC. Our results infer that the primary sensing of dsRNA in CD8α⁺ DC is competent to induce cross-presentation, which minimally involves the IPS-1 or IFNAR amplification pathway, at least at a low dose of polyI:C. Yet, subsequent induction of Type I IFN via the IFNAR may further amplify the cross-priming.[18,41] Further studies are needed as to which of the TICAM-1-inducible genes link to the cross-presentation in CD8α⁺ DC.

The main focus of this study was to identify the pathway for transversion of immature DC to the CTL-driving phenotype by co-administration of polyI:C with soluble Ag. The IPS-1 pathway, although barely participates in antitumor CTL driving, can upregulate CD40/CD86 co-stimulators on the membranes of splenic CD8α⁺ and CD8α⁻ DC in response to polyI:C, suggesting that MDA5 does function in the cytoplasm of splenic CD8α⁺ and CD8α⁻ DC to sense polyI:C. However, effective CTL induction happens only in CD8α⁺ DC when stimulated with polyI:C. CD8α⁺ DC express TLR3 but CD8α⁻ DC do not, and CD8α⁺ DC with no TLR3 fail to induce CTL, suggesting that integral co-stimulation by MDA5/IPS-1 is insufficient for DC to induce cross-priming of CD8 T cells: antitumor CTL are not induced until the TICAM-1 signal is provided in DC. At least, sole effect of the IPS-1 pathway and upregulation of co-stimulators on CD8α⁺ DC is limited for cross-priming and induction of antitumor CTL, which result partly reflects those in a previous report where IPS-1 and TICAM-1 harbor a similar potential for CD8 T cell proliferation when polyI:C (Alum-containing) is employed as an adjuvant for CD8α⁺ DC to test proliferation of anti-OVA CTL.[21]

A question is why TICAM-1 is dominant to IPS-1 for response to exogenously-added polyI:C in CD8α⁺ DC. The answer is rooted in the difference of functional behavior between BMDC and CD8α⁺ DC. TLR3 levels are variable depending upon subsets of DC,[22] which affects DC subset-specific induction of cellular immune response. The high TLR3 expression (partly surface-expressed) is situated in CD8α⁺ DC before polyI:C stimulation, which is distinct from the properties of F4/80⁺ Mf and presumably BMDC of low TLR3 expression. The polyI:C-uptake machinery[15] appears to efficiently work in concert with the TLR3/TICAM-1 pathway in CD8α⁺ DC and this tendency is diminished when CD8α⁺ DC are pretreated with Alum + polyI:C.[21] Furthermore, there are functional discrepancies between CD8α⁺ splenic DC and GM-CSF-induced BMDC, which appears to reflect the difference of their TLR3 levels.[22] These results on CD8α⁺ DC encourage us to develop dsRNA adjuvant immunotherapy supporting TAA soluble vaccines for cancer applicable to humans, which possess the counterpart of CD8α⁺ DC.

There are two modes of dsRNA-mediated DC maturation, intrinsic and extrinsic modes that are governed by the IPS-1 and TICAM-1 pathways, respectively.[9,34] It is important to elucidate the in vivo qualitative difference in the two pathways in tumor-loading mice. TLR3⁺ DC/Mf are responsible for CTL driving via an extrinsic route in viral infection.[34] Previous data suggested that dsRNA in infectious cell debris, rather than viral dsRNA produced in the cytoplasm of Ag-presenting cells or autophagosome formation, contribute to fine tuning of DC maturation through extrinsic dsRNA recognition.[16] It is reported that dsRNA-containing debris are generated secondary to infection-mediated cell death,[41] and DC phagocytose by-stander dead cells. Likewise, soluble tumor Ags released from tumor cells usually are extrinsically taken up by APC in patients with cancer.[42] If CTL are successfully induced in therapeutic biotherapy targeted against cancer cells, this extrinsic TICAM-1 pathway must be involved in the therapeutic process.

Cross-presentation occurs in a TAP-dependent[43] and -independent fashions.[44,45] The peptides are transported by TAP into the endoplasmic reticulum (ER) and loaded onto MHC Class I for presentation at the cell surface. ER and phagosome might fuse each other for accelerating cross-presentation.[46] Another possibility is that cross-presentation occurs in early endosomes where TLR3 resides. This early endosome cross-presentation does not always depend on TAP[42-44] but requires TLR stimulation.[34] TLR4/MyD88 pathway is involved in the TAP-dependent early endosome model,[43] where recruitment of TAP to the early endosomes is an essential step for the cross-presentation of soluble Ag. These models together with our genechip analysis of polyI:C-stimulated BMDC suggested that some ER-associated proteins are upregulated in BMDC by polyI:C-TICAM-1 pathway. The results infer that the TLR3/TICAM-1 rather than the TLR4/MyD88 pathway more crucially participates in cross-presentation in response to dsRNA or viral stimuli and facilitates raising CTL antitumor immunity in APC.

Although multiple RNA sensors couple with TICAM-1 and signal to activate the Type I IFN-inducing pathway,[25] at least TLR3 in the CD8α⁺ DC are critical in CTL driving. CD8α⁺ DC are a high TLR3 expresser, while BMDC express TLR3 with only low levels.[22] CD8α⁻ DC do not express it.[22] The Ag presentation and TLR3 levels in CD8α⁺ DC appear reciprocally correlated with the phagocytosing ability of DC. Although the TLR3 mRNA level is downregulated secondary to polyI:C response after maturation, this may not be related to the CD8α⁺ DC functions. Yet, polyI:C might interact with other cytoplasmic sensors for DC maturation,[32,47]

The route of administration and delivery methods may be important for culminate the polyI:C adjuvant function. The toxic problem has not overcome in the adjuvant therapy using polyI:C[35,36] and this is a critical matter for clinical introduction of dsRNA reagents to immunotherapy. The most problematic is the life-threatening shock induced by polyI:C. Recent advance of polyI:C study suggests that PEI-jet helps efficient uptake of polyI:C into peritoneal macrophages.[48] LC (poly-L-lysine and methylcellulose) has been used as a preservative to reduce the toxic effect of polyI:C.[49] Nanotechnological delivery of polyI:C results in efficient tumor regression.[50] There are many subsets of DC that can be defined by surface markers, and selecting an appropriate administration route can target a specific DC subset. The route for s.c. administration usually mature dermal/epidermal DC or Langerhans cells.[51,52] Some DC subsets with unique properties specialized to CTL induction would work in association with the route of polyI:C administration. Attempting to develop more harmless and efficient dsRNA derivatives will benefit for establishing human adjuvant immunotherapy for cancer.

Materials and Methods

Mice. TICAM-1$^{-/-}$ and IPS-1$^{-/-}$ mice were made in our laboratory and backcrossed more than eight times to adapt C57BL/6 background.[12] IRF-3/7$^{-/-}$ and IFNAR$^{-/-}$ mice were kindly provided by T. Taniguchi (University of Tokyo, Tokyo, Japan). TLR3$^{-/-}$ mice were kindly provided by S. Akira (Osaka University, Osaka, Japan). Rag2$^{-/-}$ and OT-1 mice were kindly provided from Drs N. Ishii (Tohoku University, Sendai, Japan). Rag2$^{-/-}$/OT-1 mice were bred in our laboratory. All mice were maintained under specific pathogen-free conditions in the animal facility of the Hokkaido University Graduate School of Medicine. Animal experiments were performed according to the guidelines set by the animal safety center, Hokkaido University, Japan.

Cells. EG7 and C1498 cells were purchased from ATCC and cultured in RPMI1640/10% FCS/55 μM 2-ME/1 mM sodium pyruvate and RPMI1640/10% FCS/25 ng/ml 2-ME, respectively. Mouse splenocytes, OT-1 T cell, CD8α⁺ DC and CD8α⁻ DC were harvested from the spleen and cultured in RPMI1640/10% FCS/55 μM 2-ME/10 mM HEPES.[41] B16D8 cells were cultured in RPMI/10% FCS as described previously.[12]

Reagents and antibodies. Ovalbumin (OVA) and polyI:C (polyI:C) were purchased from SIGMA and Amersham Biosciences, respectively. $OVA_{257-264}$ peptide (SIINFEKL: SL8)

©2012 Landes Bioscience. Do not distribute.

and OVA ($H2K^b$-SL8) Tetramer were from MBL. Following Abs were purchased: anti-CD3ε (145-2C11), anti-CD8β (53-6.7), anti-CD11c (N418), anti-CD16/32 (93), anti-CD69 (H1.2F3) and anti-IFNγ(XMG1.2) Abs from BioLegend, anti-B220 (RA3-6B2), anti-CD4 (L3T4), anti-CD40 (1C10), anti-CD86 (GL1), and anti-MHC I-SL8 (25-D1.16) Abs from eBiosciences, anti-TCR-Vβ5.1/5.2 Ab and ViaProbe from BD Biosciences. The Rat anti-mouse TLR3 mAb (11F8) was kindly provided by David M. Segal (National Institute of Health, Bethesda, MD). To rule out LPS contamination, we treated OVA or other reagents with 200 μg/ml of Polymixin B for 30 min at 37°C before use. Texas Red- or FITC-labeled poly(I:C) was prepared using the 5' EndTag™ Nucleic Acid Labeling System (Vector Laboratories) according to the manufacturers instructions.

Tumor challenge and poly I:C therapy. Mice were shaved at the back and s.c. injected with 200 μl of 2×10^6 syngenic EG7 cells in PBS. Tumor volumes were measured at regular intervals by using a caliper. Tumor volume was calculated by using the formula: Tumor volume (cm^3) = (long diameter) × (short diameter)^2 × 0.4. A volume of 50 μl of a mixture consisting of the lysate of 2×10^5 EG7 cells with or without 50 μg of poly I:C (polyI:C) was s.c. injected around the tumor. We added no other emulsified reagent for immunization since we want to role out the conditional effect of the Ag/polyI:C. The treatments were started when the average of tumor volumes reached at 0.4–0.8 cm^3 and performed twice per week. EG7 lysate were prepared by three times freeze/thaw cycles (-140°C/37°C) in PBS, with removal of cell debris by centrifugation at 6,000 g for 10 min.[53] To deplete CD8 T cells, mice were i.p. injected with hybridoma ascites of anti-CD8β mAb. The dose of antibody and the treatment regimens were determined in preliminary studies by using the same lots of antibody used for the experiments. Depletion of the desired cell populations by this treatment was confirmed by FACS for the entire duration of the study.

Evaluation of T cell activity in tumor-bearing mice. Draining inguinal LN cells were harvested from tumor-bearing mice after 24 h from the last polyI:C treatment. The activity of T cells was evaluated by CD69 expression and IL-2/IFNγ production. These cells were stained with FITC-CD8α, PE-CD69, PerCP/Cy5.5-7AAD and APC-CD3ε. To check cytokine production, LN cells were cultured for 3 d in vitro in the presence or absence of EG7 lysates and IL-2 and IFNγ productions were determined by Cytokine Beads Array (CBA) assay (BD). To assess the cytotoxic activity of CTL, standard ^{51}Cr release assay was performed. For CTL expansion, 2.5×10^6 LN cells were co-cultured with 1.25×10^5 mitomycin C-treated EG7 cells in the presence of 10 U/ml IL-2 for 5 d. Then, LN cells were incubated with ^{51}Cr-labeled EG7 or C1498 cells for 4 h and determined cytotoxic activity. The cell-specific cytotoxicity was calculated with subtracting the cytotoxity for C1498 from for EG7 cells.

Antigen-specific T cell expansion in vivo. Mice were i.p. immunized with 1 mg of OVA and 150 μg of poly I:C. After 7 d, spleens were homogenized and stained with FITC-CD8α and PE-OVA Tetramer for detecting OVA-specific CD8 T cell populations. For intracellular cytokine detection, splenocytes were cultured with or without 100 nM OVA peptide (SIINFEKL; SL8) for 8 h and 10 μg/ml of Brefeldin A (Sigma-Aldrich) was added to the culture in the last 4 h. Then cells were stained with PE-anti-CD8α and fixed/permeabilized with Cytofix/Cytoperm (BD Biosciences) according to manufacturer's instruction. Then, fixed/permeabilized cells were further stained with APC-anti-IFNγ. Stained cells were analyzed with FACSCalibur (BD Biosciences) and FlowJo software (Tree Star).

In vivo CTL assay. The in vivo CTL assay was performed as described.[54] In brief, WT, TICAM-$1^{-/-}$, MAVS$^{-/-}$ and IRF-$3/7^{-/-}$ mice were i.v. administered with PBS, 10 μg of OVA or OVA with 50 μg of polyI:C. After 5 d, 2×10^7 target cells (see below) were i.v. injected to other irrelevant mice and 8 h later, the OVA-specific cytotoxicity was measured by FACSCalibur. Target cells were 1:1 mixture of 2 μM SL8-pulsed, 5 μM CFSE-labeled splenocytes and SL8-unpulesed, 0.5 μM CFSE-labeled splenocytes. OVA-specific cytotoxicity was calculated with a formula: {1-(Primed [$CFSE^{high}$(%)/$CFSE^{low}$(%)]/Unprimed [$CFSE^{high}$(%)/$CFSE^{low}$(%)]} × 100.

DC preparation. DCs were prepared from spleens of mice, as described previously.[55] In brief, collagenase-digested spleen cells were treated with ACK buffer and then washed with PBS twice. Then splenocytes were positively isolated with anti-CD11c MicroBeads. $CD11c^+$ cells were acquired routinely about ≥ 80% purity. Further, to highly purify $CD8\alpha^+$ and $CD8\alpha^-$ DCs, spleen DC were stained with FITC-CD8α, PE-B220, PE/Cy7-CD11c and PerCP5.5-7AAD. $CD8\alpha^+$ or $CD8\alpha^-$ $CD11c^+B220^-$ DCs were purified on FACSAriaII (BD). The purity of the cells was ≥ 98%.

OT-1 proliferation assay. Ten micrograms of OVA with or without 50 μg of polyI:C were i.v. injected to WT, TICAM-$1^{-/-}$, IPS-$1^{-/-}$ and DKO mice. After 4 h, $CD8\alpha^+$ or $CD8\alpha^-$ DC were purified from the spleen. 2.5×10^4 $CD8\alpha^+$ or $CD8\alpha^-$ DC were co-cultured with 5×10^4 1 μM CFSE-labeled Rag$2^{-/-}$/OT-1 T cells for 3 d in 96-well round bottom plate. These cells were stained with PE-anti-TCR-Vβ5.1,5.2 and APC-anti-CD3ε and T cell proliferation was analyzed by CFSE dilution using FACSCalibur. Additionally, IFNγ in the culture supernatant was measured by CBA assay.

Statistical analysis. P-values were calculated with one-way analysis of variance (ANOVA) with Bonferroni's test. Error bars represent the SD or SEM between samples.

Disclosure of Potenial Conflicts of Interest

No potential conflicts of interest were disclosed.

Acknowledgment

We are grateful to Drs. T. Taniguchi (University Tokyo, Tokyo), N. Ishii (Tohoku University, Sendai) and D.M. Segel (NCI, Bethesda) for providing us with IRF-$3/7^{-/-}$ mice, OT-1 mice and anti-monse TLR3 mAb, respectively. Invaluable discussions about the peptide vaccine therapy with Dr. N. Satoh (Sapporo Medical University, Sapporo) are gratefully acknowledged. We thank Drs H. Takaki, J. Kasamatsu, H.H. Aly, and H. Shime in our lab for their critical comments on this study.

This work was supported in part by Grants-in-Aid from the Ministry of Education, Science, and Culture (Specified Project for Advanced Research, MEXT) and the Ministry of Health, Labor, and Welfare of Japan, and by the Takeda and the Waxmann Foundations. Financial supports by a MEXT Grant-in-Project "The Carcinogenic Spiral" is gratefully acknowledged.

Supplemental Materials

Supplemental materials may be found here:
http://www.landesbioscience.com/journals/oncoimmunology/article/19893/

References

1. Iwasaki A, Medzhitov R. Regulation of adaptive immunity by the innate immune system. Science 2010; 327:291-5; PMID:20075244; http://dx.doi.org/10.1126/science.1183021
2. Seya T, Shime H, Ebihara T, Oshiumi H, Matsumoto M. Pattern recognition receptors of innate immunity and their application to tumor immunotherapy. Cancer Sci 2010; 101:313-20; PMID:20059475; http://dx.doi.org/10.1111/j.1349-7006.2009.01442.x
3. Akira S. Toll-like receptor signaling. J Biol Chem 2003; 278:38105-8; PMID:12893815; http://dx.doi.org/10.1074/jbc.R300028200
4. Kawai T, Akira S. The roles of TLRs, RLRs and NLRs in pathogen recognition. Int Immunol 2009; 21:317-37; PMID:19246554; http://dx.doi.org/10.1093/intimm/dxp017
5. Longman RS, Braun D, Pellegrini S, Rice CM, Darnell RB, Albert ML. Dendritic-cell maturation alters intracellular signaling networks, enabling differential effects of IFN-alpha/beta on antigen cross-presentation. Blood 2007; 109:1113-22; PMID:17018853; http://dx.doi.org/10.1182/blood-2006-05-023465
6. Shinohara ML, Kim JH, Garcia VA, Cantor H. Engagement of the type I interferon receptor on dendritic cells inhibits T helper 17 cell development: role of intracellular osteopontin. Immunity 2008; 29:68-78; PMID:18619869; http://dx.doi.org/10.1016/j.immuni.2008.05.008
7. Diebold SS. Recognition of viral single-stranded RNA by Toll-like receptors. Adv Drug Deliv Rev 2008; 60:813-23; PMID:18241955; http://dx.doi.org/10.1016/j.addr.2007.11.004
8. Matsumoto M, Oshiumi H, Seya T. Antiviral responses induced by the TLR3 pathway. Rev Med Virol 2011. Epub ahead of print. PMID:21312311; http://dx.doi.org/10.1002/rmv.680
9. Yoneyama M, Fujita T. RIG-I family RNA helicases: cytoplasmic sensor for antiviral innate immunity. Cytokine Growth Factor Rev 2007; 18:545-51; PMID:17683970; http://dx.doi.org/10.1016/j.cytogfr.2007.06.023
10. Seya T, Matsumoto M. The extrinsic RNA-sensing pathway for adjuvant immunotherapy of cancer. Cancer Immunol Immunother 2009; 58:1175-84; PMID:19184005; http://dx.doi.org/10.1007/s00262-008-0652-9
11. Akazawa T, Ebihara T, Okuno M, Okuda Y, Shingai M, Tsujimura K, et al. Antitumor NK activation induced by the Toll-like receptor 3-TICAM-1 (TRIF) pathway in myeloid dendritic cells. Proc Natl Acad Sci U S A 2007; 104:252-7; PMID:17190817; http://dx.doi.org/10.1073/pnas.0605978104
12. Ebihara T, Azuma M, Oshiumi H, Kasamatsu J, Iwabuchi K, Matsumoto K, et al. Identification of a polyI:C-inducible membrane protein that participates in dendritic cell-mediated natural killer cell activation. J Exp Med 2010; 207:2675-87; PMID:21059856; http://dx.doi.org/10.1084/jem.20091573
13. Perrot I, Deauvieau F, Massacrier C, Hughes N, Garrone P, Durand I, et al. TLR3 and Rig-like receptor on myeloid dendritic cells and Rig-like receptor on human NK cells are both mandatory for production of IFN-gamma in response to double-stranded RNA. J Immunol 2010; 185:2080-8; PMID:20639488; http://dx.doi.org/10.4049/jimmunol.1000532
14. Bevan MJ. Cross-priming for a secondary cytotoxic response to minor H antigens with H-2 congenic cells which do not cross-react in the cytotoxic assay. J Exp Med 1976; 143:1283-8; PMID:1083422; http://dx.doi.org/10.1084/jem.143.5.1283
15. Datta SK, Redecke V, Prilliman KR, Takabayashi K, Corr M, Tallant T, et al. A subset of Toll-like receptor ligands induces cross-presentation by bone marrow-derived dendritic cells. J Immunol 2003; 170:4102-10; PMID:12682240
16. Schulz O, Diebold SS, Chen M, Näslund TI, Nolte MA, Alexopoulou L, et al. Toll-like receptor 3 promotes cross-priming to virus-infected cells. Nature 2005; 433:887-92; PMID:15711573; http://dx.doi.org/10.1038/nature03326
17. Kono H, Rock KL. How dying cells alert the immune system to danger. Nat Rev Immunol 2008; 8:279-89; PMID:18340345; http://dx.doi.org/10.1038/nri2215
18. Le Bon A, Etchart N, Rossmann C, Ashton M, Hou S, Gewert D, et al. Cross-priming of CD8+ T cells stimulated by virus-induced type I interferon. Nat Immunol 2003; 4:1009-15; PMID:14502286; http://dx.doi.org/10.1038/ni978
19. Bennett SR, Carbone FR, Karamalis F, Miller JF, Heath WR. Induction of a CD8+ cytotoxic T lymphocyte response by cross-priming requires cognate CD4+ T cell help. J Exp Med 1997; 186:65-70; PMID:9206998; http://dx.doi.org/10.1084/jem.186.1.65
20. Shimizu K, Kurosawa Y, Taniguchi M, Steinman RM, Fujii S. Cross-presentation of glycolipid from tumor cells loaded with alpha-galactosylceramide leads to potent and long-lived T cell mediated immunity via dendritic cells. J Exp Med 2007; 204:2641-53; PMID:17923500; http://dx.doi.org/10.1084/jem.20070458
21. Kumar H, Koyama S, Ishii KJ, Kawai T, Akira S. Cutting edge: cooperation of IPS-1- and TRIF-dependent pathways in poly IC-enhanced antibody production and cytotoxic T cell responses. J Immunol 2008; 180:683-7; PMID:18178804
22. Jelinek I, Leonard JN, Price GE, Brown KN, Meyer-Manlapat A, Goldsmith PK, et al. TLR3-specific double-stranded RNA oligonucleotide adjuvants induce dendritic cell cross-presentation, CTL responses, and antiviral protection. J Immunol 2011; 186:2422-9; PMID:21242525; http://dx.doi.org/10.4049/jimmunol.1002845
23. Wang Y, Cella M, Gilfillan S, Colonna M. Cutting edge: polyinosinic:polycytidylic acid boosts the generation of memory CD8 T cells through melanoma differentiation-associated protein 5 expressed in stromal cells. J Immunol 2010; 184:2751-5; PMID:20164430; http://dx.doi.org/10.4049/jimmunol.0903201
24. Carbone FR, Bevan MJ. Induction of ovalbumin-specific cytotoxic T cells by in vivo peptide immunization. J Exp Med 1989; 169:603-12; PMID:2784478; http://dx.doi.org/10.1084/jem.169.3.603
25. Asano J, Tada H, Onai N, Sato T, Horie Y, Fujimoto Y, et al. Nucleotide oligomerization binding domain-like receptor signaling enhances dendritic cell-mediated cross-priming in vivo. J Immunol 2010; 184:736-45; PMID:20008287; http://dx.doi.org/10.4049/jimmunol.0900726
26. McCartney S, Vermi W, Gilfillan S, Cella M, Murphy TL, Schreiber RD, et al. Distinct and complementary functions of MDA5 and TLR3 in poly(I:C)-mediated activation of mouse NK cells. J Exp Med 2009; 206:2967-76; PMID:19995959; http://dx.doi.org/10.1084/jem.20091181
27. Watanabe A, Tatematsu M, Saeki K, Shibata S, Shime H, Yoshimura A, et al. Raftlin is involved in the nucleocapture complex to induce poly(I:C)-mediated TLR3 activation. J Biol Chem 2011; 286:10702-11; PMID:21266579; http://dx.doi.org/10.1074/jbc.M110.185793
28. Itoh K, Watanabe A, Funami K, Seya T, Matsumoto M. The clathrin-mediated endocytic pathway participates in dsRNA-induced IFN-beta production. J Immunol 2008; 181:5522-9; PMID:18832709
29. Talmadge JE, Adams J, Phillips H, Collins M, Lenz B, Schneider M, et al. Immunomodulatory effects in mice of polyinosinic-polycytidylic acid complexed with poly-L-lysine and carboxymethylcellulose. Cancer Res 1985; 45:1058-65; PMID:3155990
30. Conforti R, Ma Y, Morel Y, Paturel C, Terme M, Viaud S, et al. Opposing effects of toll-like receptor (TLR3) signaling in tumors can be therapeutically uncoupled to optimize the anticancer efficacy of TLR3 ligands. Cancer Res 2010; 70:490-500; PMID:20068181; http://dx.doi.org/10.1158/0008-5472.CAN-09-1890
31. Kaiser WJ, Offermann MK. Apoptosis induced by the toll-like receptor adaptor TRIF is dependent on its receptor interacting protein homotypic interaction motif. J Immunol 2005; 174:4942-52; PMID:15814722
32. Zhang Z, Kim T, Bao M, Facchinetti V, Jung SY, Ghaffari AA, et al. DDX1, DDX21, and DHX36 helicases form a complex with the adaptor molecule TRIF to sense dsRNA in dendritic cells. Immunity 2011; 34:866-78; PMID:21703541; http://dx.doi.org/10.1016/j.immuni.2011.03.027
33. Gitlin L, Barchet W, Gilfillan S, Cella M, Beutler B, Flavell RA, et al. Essential role of mda-5 in type I IFN responses to polyriboinosinic:polyribocytidylic acid and encephalomyocarditis picornavirus. Proc Natl Acad Sci U S A 2006; 103:8459-64; PMID:16714379; http://dx.doi.org/10.1073/pnas.0603082103
34. Matsumoto M, Seya T. TLR3: interferon induction by double-stranded RNA including poly(I:C). Adv Drug Deliv Rev 2008; 60:805-12; PMID:18262679; http://dx.doi.org/10.1016/j.addr.2007.11.005

©2012 Landes Bioscience. Do not distribute.

©2012 Landes Bioscience. Do not distribute.

35. Absher M, Stinebring WR. Toxic properties of a synthetic double-stranded RNA. Endotoxin-like properties of poly I. poly C, an interferon stimulator. Nature 1969; 223:715-7; PMID:5805520; http://dx.doi.org/10.1038/223715a0
36. Berry LJ, Smythe DS, Colwell LS, Schoengold RJ, Actor P. Comparison of the effects of a synthetic polyribonucleotide with the effects of endotoxin on selected host responses. Infect Immun 1971; 3:444-8; PMID:16557994
37. Sasai M, Shingai M, Funami K, Yoneyama M, Fujita T, Matsumoto M, et al. NAK-associated protein 1 participates in both the TLR3 and the cytoplasmic pathways in type I IFN induction. J Immunol 2006; 177:8676-83; PMID:17142768
38. Ishikawa H, Barber GN. STING is an endoplasmic reticulum adaptor that facilitates innate immune signalling. Nature 2008; 455:674-8; PMID:18724357; http://dx.doi.org/10.1038/nature07317
39. Taniguchi T, Takaoka A. A weak signal for strong responses: interferon-alpha/beta revisited. Nat Rev Mol Cell Biol 2001; 2:378-86; PMID:11331912; http://dx.doi.org/10.1038/35073080
40. Ogasawara S, Yano H, Momosaki S, Akiba J, Nishida N, Kojiro S, et al. Growth inhibitory effects of IFN-beta on human liver cancer cells in vitro and in vivo. J Interferon Cytokine Res 2007; 27:507-16; PMID: 17572015; http://dx.doi.org/10.1089/jir.2007.0183
41. Ebihara T, Shingai M, Matsumoto M, Wakita T, Seya T. Hepatitis C virus-infected hepatocytes extrinsically modulate dendritic cell maturation to activate T cells and natural killer cells. Hepatology 2008; 48:48-58; PMID:18537195; http://dx.doi.org/10.1002/hep.22337
42. Chaput N, Conforti R, Viaud S, Spatz A, Zitvogel L. The Janus face of dendritic cells in cancer. Oncogene 2008; 27:5920-31; PMID:18836473; http://dx.doi.org/10.1038/onc.2008.270
43. Burgdorf S, Schölz C, Kautz A, Tampé R, Kurts C. Spatial and mechanistic separation of cross-presentation and endogenous antigen presentation. Nat Immunol 2008; 9:558-66; PMID:18376402; http://dx.doi.org/10.1038/ni.1601
44. Shen L, Sigal LJ, Boes M, Rock KL. Important role of cathepsin S in generating peptides for TAP-independent MHC class I crosspresentation in vivo. Immunity 2004; 21:155-65; PMID:15308097; http://dx.doi.org/10.1016/j.immuni.2004.07.004
45. Kurotaki T, Tamura Y, Ueda G, Oura J, Kutomi G, Hirohashi Y, et al. Efficient cross-presentation by heat shock protein 90-peptide complex-loaded dendritic cells via an endosomal pathway. J Immunol 2007; 179:1803-13; PMID:17641047
46. Gagnon E, Duclos S, Rondeau C, Chevet E, Cameron PH, Steele-Mortimer O, et al. Endoplasmic reticulum-mediated phagocytosis is a mechanism of entry into macrophages. Cell 2002; 110:119-31; PMID:12151002; http://dx.doi.org/10.1016/S0092-8674(02)00797-3
47. Samuel CE. Antiviral actions of interferons. Clin Microbiol Rev 2001; 14:778-809; PMID:11585785; http://dx.doi.org/10.1128/CMR.14.4.778-809.2001
48. Wu CY, Yang HY, Monie A, Ma B, Tsai HH, Wu TC, et al. Intraperitoneal administration of poly(I:C) with polyethylenimine leads to significant antitumor immunity against murine ovarian tumors. Cancer Immunol Immunother 2011; 60:1085-96; PMID:21526359; http://dx.doi.org/10.1007/s00262-011-1013-7
49. Longhi MP, Trumpfheller C, Idoyaga J, Caskey M, Matos I, Kluger C, et al. Dendritic cells require a systemic type I interferon response to mature and induce CD4+ Th1 immunity with poly IC as adjuvant. J Exp Med 2009; 206:1589-602; PMID:19564349; http://dx.doi.org/10.1084/jem.20090247
50. Kitano S, Kageyama S, Nagata Y, Miyahara Y, Hiasa A, Naota H, et al. HER2-specific T-cell immune responses in patients vaccinated with truncated HER2 protein complexed with nanogels of cholesteryl pullulan. Clin Cancer Res 2006; 12:7397-405; PMID:17189412; http://dx.doi.org/10.1158/1078-0432.CCR-06-1546
51. Kushwah R, Hu J. Complexity of dendritic cell subsets and their function in the host immune system. Immunology 2011; 133:409-19; PMID:21627652; http://dx.doi.org/10.1111/j.1365-2567.2011.03457.x
52. Asano K, Nabeyama A, Miyake Y, Qiu CH, Kurita A, Tomura M, et al. CD169-positive macrophages dominate antitumor immunity by crosspresenting dead cell-associated antigens. Immunity 2011; 34: 85-95; PMID:21194983; http://dx.doi.org/10.1016/j.immuni.2010.12.011
53. Galea-Lauri J, Wells JW, Darling D, Harrison P, Farzaneh F. Strategies for antigen choice and priming of dendritic cells influence the polarization and efficacy of antitumor T-cell responses in dendritic cell-based cancer vaccination. Cancer Immunol Immunother 2004; 53:963-77; PMID:15146294; http://dx.doi.org/10.1007/s00262-004-0542-8
54. Durand V, Wong SY, Tough DF, Le Bon A. Shaping of adaptive immune responses to soluble proteins by TLR agonists: a role for IFN-α/β. Immunol Cell Biol 2004; 82:596-602; PMID:15550117; http://dx.doi.org/10.1111/j.0818-9641.2004.01285.x
55. Yamazaki S, Okada K, Maruyama A, Matsumoto M, Yagita H, Seya T. TLR2-dependent induction of IL-10 and Foxp3+ CD25+ CD4+ regulatory T cells prevents effective anti-tumor immunity induced by Pam2 lipopeptides in vivo. PLoS One 2011; 6:e18833; PMID:21533081; http://dx.doi.org/10.1371/journal.pone.0018833

©2012 Landes Bioscience. Do not distribute.

REVIEW

OncoImmunology 1:6, 917-923; September 2012; © 2012 Landes Bioscience

TLR3/TICAM-1 signaling in tumor cell RIP3-dependent necroptosis

Tsukasa Seya,* Hiroaki Shime, Hiromi Takaki, Masahiro Azuma, Hiroyuki Oshiumi and Misako Matsumoto

Department of Microbiology and Immunology; Hokkaido University Graduate School of Medicine; Sapporo, Japan

Keywords: interferon-inducing pathway, necroptosis, RIP signaling, TLR3, TICAM-1, TLR3, TRIF

Abbreviations: CTL, cytotoxic T lymphocyte; DAI, DNA-dependent activator of IFN-regulatory factors; DAMP, damage-associated molecular pattern; HMGB1, high-mobility group box 1; HSP, heat shock protein; mDC, myeloid dendritic cell; NK, natural killer; NLR, NOD-like receptor; PAMP, pathogen- associated molecular pattern; PRR, pattern-recognition receptor; RIP, receptor-interacting protein kinase; TICAM-1, Toll-IL-1-homology domain-containing adaptor molecule 1; TLR, Toll-like receptor; TNFα, tumor necrosis factor α; TNFR1, TNFα receptor 1

The engagement of Toll-like receptor 3 (TLR3) leads to the oligomerization of the adaptor TICAM-1 (TRIF), which can induces either of three acute cellular responses, namely, cell survival coupled to Type I interferon production, or cell death, via apoptosis or necrosis. The specific response elicited by TLR3 determines the fate of affected cells, although the switching mechanism between the two cell death pathways in TLR3-stimulated cells remains molecularly unknown. Tumor necrosis factor α (TNFα)-mediated cell death can proceed via apoptosis or via a non-apoptotic pathway, termed necroptosis or programmed necrosis, which have been described in detail. Interestingly, death domain-containing kinases called receptor-interacting protein kinases (RIPs) are involved in the signaling pathways leading to these two cell death pathways. Formation of the RIP1/RIP3 complex (called necrosome) in the absence of caspase 8 activity is crucial for the induction of necroptosis in response to TNFα signaling. On the other hand, RIP1 is known to interact with the C-terminal domain of TICAM-1 and to modulate TLR3 signaling. In macrophages and perhaps tumor cell lines, RIP1/RIP3-mediated necroptotic cell death can ensue the administration of the TLR agonist polyI:C. If this involved the TLR3/TICAM-1 pathway, the innate sensing of viral dsRNA would be linked to cytopathic effects and to persistent inflammation, in turn favoring the release of damage-associated molecular patterns (DAMPs) in the microenvironment. Here, we review accumulating evidence pointing to the involvement of the TLR3/TICAM-1 axis in tumor cell necroptosis and the subsequent release of DAMPs.

Introduction

Cell death is an important process for both development and homeostasis in multicellular organisms. The mode of cell death is closely associated with other biological responses occurring within the host, including inflammation. Cell death has been categorized as apoptotic or necrotic and, until recently, apoptosis had been considered as a synonym of programmed cell death.[1] Caspases are a family of cysteine proteases that mediate apoptotic cell death in response to ligands of death receptors, including tumor necrosis factor α (TNFα), FAS ligand (FASL) and TRAIL, as well as to intracellular damage, upon the induction of pro-apoptotic BH3-only members of the Bcl-2 family. However, it is now clear that apoptosis is not the only cellular mechanism that mediates programmed cell death. Necrotic cell death, which has traditionally been viewed as a form of passive cell death, may also be regulated, and in this case has been called necroptosis or programmed necrosis.[2] Necroptosis may be induced by TNFα receptor 1 (TNFR1) agonists, but also by innate pattern-recognition receptors (PRRs) such as Toll-like receptor (TLR) 3 and TLR4.[1,4] These two TLRs can recruit the adaptor TICAM-1 (also known as TRIF), leading to Type I interferon (IFN) signaling.[3] In line with this notion, the TLR3 ligand polyI:C (a synthetic double-stranded RNA, dsRNA) can activate either apoptosis or necrosis, depending on the cell lines tested. Cell death induced by the TLR3-TICAM-1 axis may therefore be executed through two distinct subroutines.[5] The mechanisms that dictate the cellular decision to undergo apoptosis or necroptosis in response to TLR3 signaling, as well as the mechanisms that mediate the execution of necroptosis, are the subject of intense investigation.

Toll-like receptors and other PRRs harbor the ability to specifically recognize microbial molecules, known as pathogen-associated molecular patterns (PAMPs).[6] PAMPs trigger the maturation of myeloid dendritic cells (mDCs) through the activation of TLR and/or other pathways, eventually eliciting cellular immunity.[7] In mDCs, nucleic acid-recognizing TLRs (i.e., TLR3, TLR7, TLR8 and TLR9) reside in endosomes and sense their ligands only when they are internalized.[8] The uptake of DNA or RNA of microbial origin therefore allows cross-presentation to T cells and the exposure of natural killer (NK) cell-activating ligands. Besides this extrinsic maturation route, it is known that the formation of autophagosomes may deliver cytoplasmic nucleic acids of viral origin to the endosome via autophagy.[9] In either route, TLR signaling links immunological events to pathological cell death.

Recently accumulated evidence suggests that TLRs serve as receptors not only for foreign PAMPs but also for cellular

*Correspondence to: Tsukasa Seya; Email: seya-tu@pop.med.hokudai.ac.jp
Submitted: 05/28/12; Accepted: 06/22/12
http://dx.doi.org/10.4161/onci.21244